# 13 Crustal Exhumation of Plutonic and Metamorphic Rocks: Constraints from Fission-Track Thermochronology

Suzanne L. Baldwin, Paul G. Fitzgerald and Marco G. Malusà

**Abstract**

The thermal evolution of plutonic and metamorphic rocks in the upper crust may be revealed using fission-track (FT) analyses and other low-temperature thermochronologic methods. The segment of pressure–temperature–time–deformation (*P-T-t-D*) rock paths potentially constrained by FT data corresponds to the lower greenschist facies, prehnite–pumpellyite, and zeolite facies of metamorphic rocks and also includes regions where diagenetic alteration occurs. When plutonic and metamorphic rocks are exhumed, thermal perturbations caused by fluid alteration, and crystallisation below relevant closure/annealing temperatures at relatively shallow crustal depths, may preclude a simplistic interpretation of thermochronologic ages in terms of monotonic cooling. However, FT ages and track-length measurements provide kinetic data that allow interpretation of *T-t* paths, even in cases where assumptions based on bulk closure temperatures are violated. We show that geologically well-constrained sampling strategies, and application of multiple thermochronologic methods on cogenetic minerals from plutonic and metamorphic rocks, may provide the most promising means to document the timing, rates, and mechanisms of crustal processes. Case studies are presented for: (1) (ultra)high-pressure (U)HP metamorphic terranes (e.g., Papua New Guinea, Western Alps, Western Gneiss Region, Dabie–Sulu), (2) an extensional orogen (Transantarctic Mountains), (3) a compressional orogen (Pyrenees), and (4) a transpressional plate boundary zone (Alpine fault zone, New Zealand).

S. L. Baldwin (✉) · P. G. Fitzgerald
Department of Earth Sciences Syracuse University, Syracuse, NY 13244, USA
e-mail: sbaldwin@syr.edu

M. G. Malusà
Department of Earth and Environmental Sciences, University of Milano-Bicocca, Piazza Delle Scienza 4, 20126 Milan, Italy

## 13.1 Introduction

Plutonic and metamorphic rocks form at depth beneath the Earth's surface. Plutonic rocks crystallise at depth from magmas (i.e., silicate melts). Prior to crystallising, magmas transport heat and mass by flow at temperatures and pressures that depend upon the magma's bulk composition. Crystallisation involves both nucleation and crystal growth processes, with rates dependent upon the temperature–time (*T-t*) history. In contrast, metamorphic rocks form by solid-state crystallisation of protoliths (igneous, metamorphic or sedimentary rocks) that have been subjected to changes in temperatures and pressures. Metamorphic minerals and their textures change primarily in response to temperature that together with available fluids drive metamorphic reactions. The result is that original mineral assemblages may be transformed to more stable assemblages at new pressure and temperature conditions.

Major perturbations of crustal geothermal gradients are required to form igneous and metamorphic rocks, so it cannot be assumed a priori that these rocks achieved equilibrium as a result of steady-state conditions (e.g., Spear 1993). In active plate boundary zones, where most igneous and metamorphic rocks form, geothermal gradients are spatially complex and change as plate boundaries evolve. Transient geothermal gradients result from heat sources (e.g., intruding magmas, exothermic reactions) and heat sinks (subducting slabs, endothermic reactions). For example, at divergent plate boundaries rising asthenosphere causes decompression melting, which results in steepening of the geothermal gradient and high-temperature metamorphism of the country rock. At convergent plate boundaries, subducting cold lithosphere leads to high-*P*/low-*T* metamorphism and results in low geothermal gradients relative to steady-state geothermal gradients (Fig. 13.1a). If active deformation is associated with rapid exhumation, geothermal gradients are likely to change due to heat advection as rocks move rapidly from depth towards the surface. Our ability to



M. G. Malusà and P. G. Fitzgerald (eds.), *Fission-Track Thermochronology and its Application to Geology*,
Springer Textbooks in Earth Sciences, Geography and Environment, https://doi.org/10.1007/978-3-319-89421-8_13

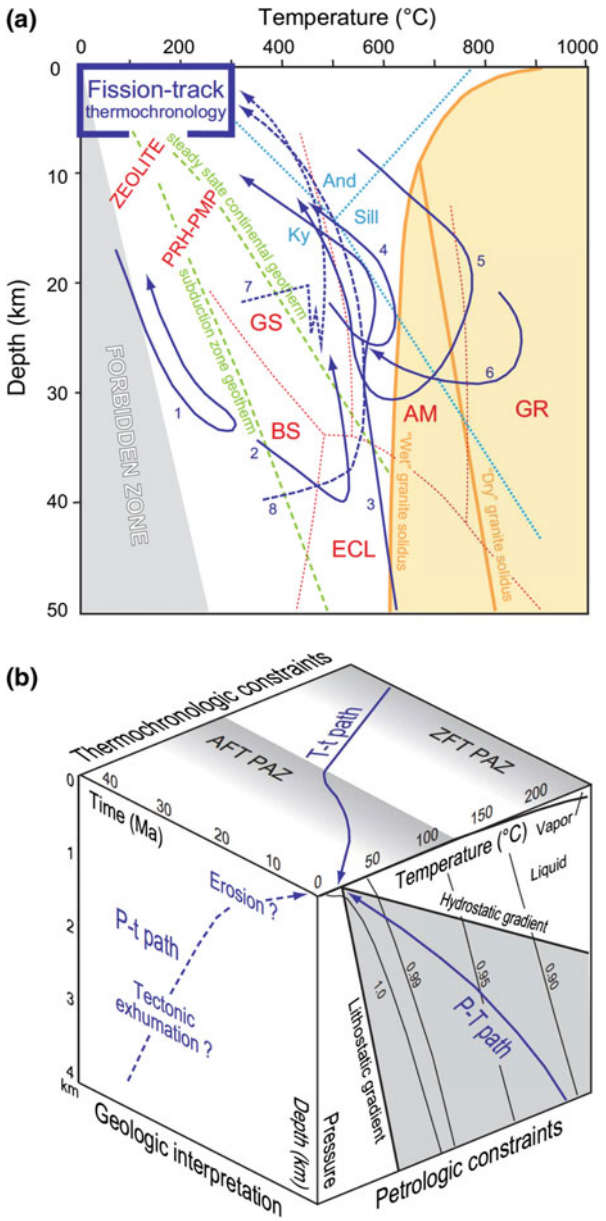


**Fig. 13.1** **a** Depth–temperature diagram showing examples of *P-T* paths for metamorphic rocks (in blue) (after Philpotts and Ague 2009): 1, Franciscan Complex (Ernst 1988); 2, Western Alps (Ernst 1988); 3, Dora-Maira (Rubatto and Hermann 2001); 4 and 5, central Massachusetts (Tracy and Robinson 1980); 6, Adirondacks, NY (Bohlen et al. 1985); 7 and 8, upper and lower units of the Tauern window, Eastern Alps (Selverstone et al. 1984; Selverstone and Spear 1985). Note that the lowest temperature parts of all *P-T* paths are not constrained. Blue box indicates *P-T* space relevant for constraining histories using FT thermochronology. Metamorphic facies (in red): AM, amphibolite; BS, blueschist; ECL, eclogite; GR, granulite; GS, greenschist; PRH-PMP, prehnite–pumpellyite. Reaction curves for $Al_2SiO_5$, wet and dry solidi indicated by light blue dotted lines. **b** *T-t-depth* space for rock *P-T-t* paths corresponding to very low grade and diagenetic conditions. *P(depth)-T* conditions are determined from fluid inclusions (lines of constant density for the $H_2O$ system, in g/cm$^3$, after Goldstein and Reynolds 1994). The hypothetical *T-t* path includes ZFT and AFT with partial annealing zones (PAZ) indicated. The dashed line on the left-hand panel shows an example of a *P(depth)-t* path associated with shallow crustal exhumation mechanisms

constrain crustal exhumation histories of plutonic and metamorphic rocks largely depends on our understanding of the dynamic thermal reference frame used to interpret thermochronologic data (see Chap. 8, Malusà and Fitzgerald 2018a) and an understanding of the range of chemical and physical processes that can potentially affect plutonic and metamorphic rocks during exhumation.

This chapter discusses the final exhumation paths of plutonic and metamorphic rocks, as they make their way to the surface, and the importance of using FT thermochronology to constrain and quantify the timescales, rates, and mechanisms of crustal motion on geologic timescales. It is written from a "rock exhumation trajectory" perspective, following plutonic and metamorphic rocks from deep crustal levels where constraints on exhumation are generally obtained using high-temperature thermochronologic techniques and petrologic data, towards shallow crustal levels where low-temperature thermochronologic techniques are applicable. There are many common assumptions associated with techniques used to constrain exhumation from deep crustal levels as compared to those used to constrain exhumation from shallow crustal levels. However, important differences exist, such as the role of mineral (re)crystallisation in the deep crust versus the influence of topography on isotherms at shallow crustal levels. We present case studies from different tectonic settings to illustrate how FT thermochronology on minerals from metamorphic and plutonic rocks can be interpreted within a geologic framework. Our synthesis takes into account potential complications due to processes (e.g., heat advection, hydrothermal alteration) that may affect rocks during crustal exhumation.

## 13.2 Thermochronologic Data Interpretation of Plutonic and Metamorphic Rocks

### 13.2.1 An Integrated Approach to P-T-t-D Path Determination

Mineral assemblages and textures preserved in plutonic and metamorphic rocks provide a record of changing pressure (*P*), temperature (*T*), and deformation (D) during transit from depth to the surface. Mineral assemblages and textures are a function of bulk rock compositions, rheology, volatile contents, and *P-T* conditions. Principles of physical chemistry and phase equilibria applied to natural rocks and synthetic materials by experimentalists and thermodynamic modellers allow petrologists to assess *P-T* conditions (e.g., Spear 1993; Powell and Holland 2010; Sawyer et al. 2011). A rock's *P-T* path can be constructed by connecting regions in *P-T* space where the stability of mineral assemblages, compositions, or changes in compositions (e.g., in the case of zoned minerals), and their textures, are known (e.g., Spear

1993). Reactions used to quantify metamorphic pressures and temperatures typically occur diachronously, and radiometric dating techniques can be applied to minerals to determine the ages associated with segments of the *P-T* paths (Fig. 13.1a). Thermobarometric data provided by petrologic analysis and *T-t* information provided by thermochronology can be integrated to define *P-T-t* paths that shed light on geologic processes controlling crustal rock exhumation (e.g., Baldwin and Harrison 1992; Duchêne et al. 1997; Malusà et al. 2011; Baldwin 1996).

Accessory phases have proven especially useful for linking isotopic ages to petrologic and textural information (e.g., Kohn 2016). Most radiometric data (Rb–Sr, $^{40}Ar/^{39}Ar$, U–Pb, Sm–Nd, Lu–Hf) can be interpreted with respect to mineral (re)crystallisation to infer the timing and rates of crustal processes such as metamorphism and ductile deformation. Field, macro-, micro-, and nano-structural analysis provide the structural context required for correlating mineral assemblages from different outcrops and to add rheologic constraints in the construction of *P-T-t-D* paths. In the low-temperature range—corresponding to the lower greenschist, prehnite–pumpellyite, and zeolite facies of metamorphic rocks and including diagenesis—time constraints provided by FT thermochronology are particularly useful to define the final portion of the exhumation path (Fig. 13.1b) (e.g., Malusà et al. 2006). However, many published exhumation paths do not incorporate data that allow paths to be extended to the lowest temperature ranges (Fig. 13.1a). In such cases, information, potentially provided by full integration of petrologic and thermochronologic data sets, remains unexploited.

### 13.2.2 Processes, Timescales, and Rates

If it can be demonstrated that rocks cooled monotonically from high to low temperatures, and minerals represent equilibrium assemblages, application of geothermometers and thermochronometers with equilibration temperatures equal to isotopic closure temperatures ($T_c$) can be simply applied (e.g., Hodges 1991). However, petrologic evidence, such as mineral inclusion suites, mineral zoning patterns, and microstructures often reveals that equilibrium has not been achieved during exhumation, rendering thermochronologic interpretations based on simple $T_c$ models invalid. During transit to the surface, most minerals in plutonic and metamorphic rocks only partially retain their radiogenic daughter nuclides, either due to metamorphic (re) crystallisation which is often accompanied by deformation or due to diffusive loss of radiogenic daughter products. Therefore, knowledge of the minerals' petrogenesis provides constraints on rate-limiting daughter product loss mechanisms (e.g., volume diffusion, dissolution/precipitation, syn-kinematic recrystallisation) and aids in thermochronologic data interpretation. Because apatite FT (AFT) thermochronology is usually interpreted with respect to temperatures less than ~120 °C, and zircon FT (ZFT) thermochronology less than ~300 °C, taking into account (re)crystallisation of minerals within these temperature ranges is often neglected in AFT and ZFT thermochronologic data interpretation. However, metamorphic rims can form on pre-existing zircons at temperatures as low as ~250 °C (e.g., Rasmussen 2005; Hay and Dempster 2009) complicating isotopic data interpretation on zircons with demonstrable growth zones (Zirakparvar et al. 2014). Especially in cases where FT data are integrated with U–Pb ages, zircon petrogenesis must be known to ensure accurate geologic interpretations are made.

Distinguishing between the timing of mineral and rock formation, and cooling related to exhumation, is particularly important for the analysis of plutonic and metamorphic rocks. Timescales for magmatic cooling may range over orders of magnitude, from millions of years (e.g., in the case of slowly cooled batholiths) to <100,000 years (e.g., Petford et al. 2000). Modelled timescales of regional metamorphism during continent–continent collision (e.g., England and Thompson 1984) are orders of magnitude greater than timescales derived from garnet growth zones based on diffusion modelling (e.g., Dachs and Proyer 2002; Ague and Baxter 2007; Spear 2014) and from numerical modelling of thermochronologic data (e.g., Camacho et al. 2005; Viete et al. 2011). Short-lived orogenic events (<1 Myr; Dewey 2005) may result in rapid rock exhumation at rates comparable to plate tectonic rates (i.e., cm/year; e.g., Zeitler et al. 1993; Rubatto and Hermann 2001; Baldwin et al. 2004).

### 13.2.3 Approaches Used to Determine Rock Exhumation Rates

Two approaches have commonly been used to determine exhumation rates from thermochronologic data (e.g., Purdy and Jager 1976; Blythe 1998; McDougall and Harrison 1999 and references therein). These are generally known as the multiple method and age–elevation approaches (see Chap. 10, Malusà and Fitzgerald 2018b). The first approach utilises multiple thermochronologic methods applied to minerals from the same sample. Cooling rates are calculated using differences in bulk $T_c$ divided by the difference in apparent ages corresponding to the minerals analysed. Cooling rates are then converted to exhumation rates assuming a geothermal gradient. This bulk closure temperature approach—interpolation of *T-t* points obtained from analyses and assuming a nominal $T_c$ (Dodson 1973)—has many built-in assumptions which are usually violated when considering the exhumation of metamorphic and plutonic rocks (e.g., Harrison and Zeitler 2005). Assumptions

made when using this approach include: (a) diffusion is the loss mechanism operative over geologic time, (b) kinetic parameters are known, and (c) geothermal gradients remained constant and/or are known during the time period investigated.

The second common approach involves age determination on a suite of samples collected over a large elevation range (i.e., "vertical profiles"; see Chap. 9; Fitzgerald and Malusà 2018). The simple interpretation of the slope on an age–elevation profile is that it represents an apparent exhumation rate. However, due to advection of isotherms and topographic effects, the slope on an age–elevation profile typically provides an overestimate of the exhumation rate (e.g., Gleadow and Brown 2000; Braun 2002; Huntington et al. 2007). In some cases, the age–elevation profile may reveal an exhumed partial annealing zone (PAZ) or partial retention zone (PRZ). In these cases, a distinctive break in slope is interpreted to mark the base of a former PAZ/PRZ, and the slope below the break in slope marks an increase in cooling rate, usually associated with an increase in exhumation rate (see Chap. 9; Fitzgerald and Malusà 2018). In AFT thermochronology, ages and track-length distributions are used to determine thermal histories and cooling rates (see Chap. 3; Ketcham 2018). Modelled AFT thermal histories can be extended to higher temperatures through integration of modelled $^{40}Ar/^{39}Ar$ step heat data on cogenetic K-feldspar (e.g., Lovera et al. 2002; see examples below).

## 13.3 Application of FT Thermochronology to the Exhumation of (U)HP Terranes

Blueschist and eclogite-facies metamorphic rocks form when lithosphere is subducted faster than it can thermally equilibrate, and isotherms are depressed leading to characteristic high-*P/T* geothermal gradients (Fig. 13.1a). The discovery of coesite (the high-pressure $SiO_2$ polymorph) in eclogite-facies metamorphic rocks (Chopin 1984; Smith 1984) led to development of the field of UHP metamorphism (e.g., Coleman and Wang 1995; Hacker 2006; Gilotti 2013). Evidence of UHP metamorphism has been documented in more than twenty terranes, in regions of present or former plate convergence (e.g., Guillot et al. 2009; Liou et al. 2009). It is now accepted that UHP rocks form when oceanic and continental lithosphere is subducted to mantle depths, as confirmed by geophysical evidence (Zhao et al. 2015; Kufner et al. 2016). However, there is no consensus concerning how UHP rocks are exhumed from mantle depths to the surface (e.g., Malusà et al. 2015; Ducea 2016 and references therein).

Low-temperature thermochronology usually constrains rock exhumation from shallow crustal levels. Since the final stage of (U)HP exhumation may occur tens or hundreds of millions of years after the main exhumation phase (i.e., from mantle depths), low-temperature thermochronologic ages may not necessarily be interpreted relative to the timing of (U)HP exhumation, especially in the case of pre-Cenozoic UHP terranes (Fig. 13.2b). We emphasise that the timing of final exhumation within the subduction channel, as constrained by FT data, is essential for an accurate tectonic interpretation of petrologic and thermochronologic data from subduction complexes. Depending upon the paleogeothermal gradients, AFT ages may correspond to the timing of cooling and exhumation from depths ranging from ~15 km (e.g., in the case of syn-subduction exhumation with gradients of 10 °C/km) to ~4 km (e.g., in the case of post-subduction exhumation with gradients of ~30 °C/km). Independent constraints on paleogeothermal gradients (see Chap. 8, Malusà and Fitzgerald 2018a, b) are thus crucial for a reliable analysis of (U)HP rock exhumation. FT thermochronology may also be used to determine when different lithologic units (e.g., comprising a tectonic mélange) are amalgamated to form a composite terrane. Below, we summarise low-temperature constraints on (U)HP terranes and explain why these data are essential to assess timing, rates, and mechanisms of final (U)HP rock exhumation.

### 13.3.1 Cenozoic (U)HP Terranes

Eastern Papua New Guinea (PNG) and the Western Alps are among the best-studied examples of Cenozoic (U)HP terranes. The PNG (U)HP terrane is exhuming in a region of active rifting within the obliquely convergent Australian–Woodlark plate boundary zone (Baldwin et al. 2004, 2008). Domes of high-grade migmatitic gneisses (e.g., Davies and Warren 1988; Gordon et al. 2012), comprised of protoliths derived largely from Australian continental crust (Zirakparvar et al. 2012), are separated from oceanic lithospheric fragments by mylonitic shear-zone carapace (e.g., Hill et al. 1992; Little et al. 2007). Seismically active normal faults flank the domes (e.g., Abers et al. 2016) and are interpreted to have formed within an accretionary wedge along the former subduction thrust now marked by serpentinite (e.g., Baldwin et al. 2012). The location of intermediate depth earthquakes in proximity to exhumed coesite eclogite (Abers et al. 2016) suggests that rock exhumation from UHP depths may be ongoing. The timing of UHP metamorphism in eastern PNG (~7–8 Ma) is based on concordant ages obtained on cogenetic minerals from coesite eclogite using three methods: in situ zircon ion probe U–Pb (Monteleone et al. 2007), garnet Lu–Hf (Zirakparvar et al. 2011), and phengite $^{40}Ar/^{39}Ar$ (Baldwin and Das 2015). Most metamorphic zircon growth occurred during exhumation (Monteleone et al. 2007; Gordon et al. 2012; Zirakparvar et al. 2014) as confirmed by zircon petrologic models (Kohn et al.

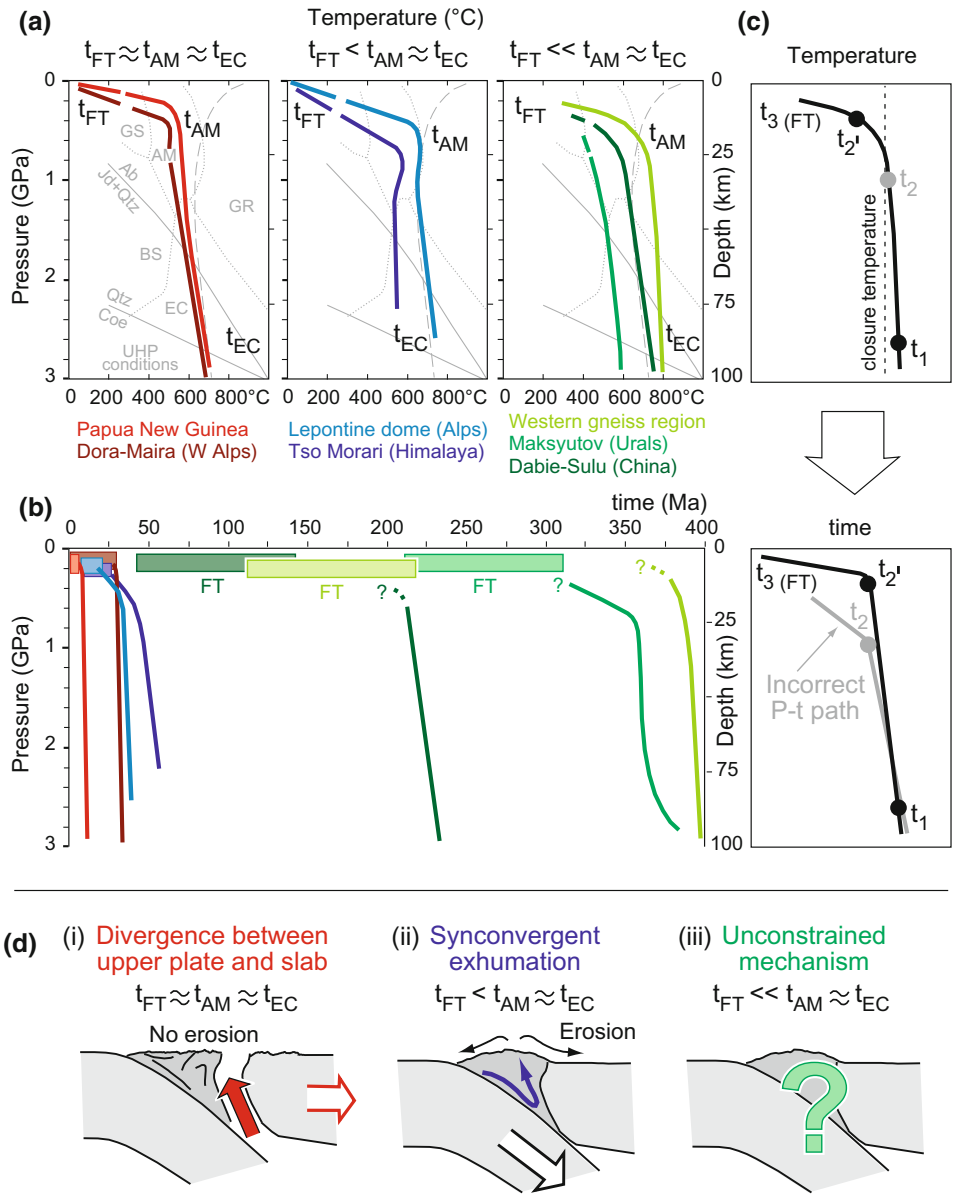


**Fig. 13.2** **a** Schematic *P-T* plots for selected UHP terranes, with colours corresponding to terranes indicated: Papua New Guinea (Baldwin and Das 2015), Dora-Maira (Chopin et al. 1991; Gebauer et al. 1997; Rubatto and Hermann 2001), Lepontine (Becker 1993; Gebauer 1996; Brouwer et al. 2004; Nagel 2008), Tso Morari (de Sigoyer et al. 2000; Schlup et al. 2003), Western Gneiss Region (Rohrman et al. 1995; Carswell et al. 2003; Kzienzyk et al. 2014), Maksyutov (Lennykh et al. 1995; Leech and Stockli 2000), Dabie–Sulu (Reiners et al. 2003; Hu et al. 2006; Liou et al. 2009); $t_{FT}$ indicates age constraints based on FT analysis. Timing of amphibolite facies metamorphism ($t_{AM}$), timing of eclogite-facies metamorphism ($t_{EC}$) based on U–Pb, $^{40}Ar/^{39}Ar$, and Lu–Hf isotopic data. **b** Schematic *P-t* paths of UHP terranes to illustrate differences in the length of time associated with final exhumation to the surface relative to the timing of UHP metamorphism. **c** Upper panel: schematic *P-T* paths (shown in black) illustrate the importance of having geobarometric constraints associated with exhumation paths. The timing of peak UHP conditions ($t_1$), retrograde overprint ($t_2$ and $t_{2'}$), and final exhumation ($t_3$(FT)) based on FT analyses. $t_{2'}$ is the age recorded by a mineral at low P conditions as a result of a late syn-kinematic recrystallisation event (e.g., a late greenschist facies foliation marked by micas) or of a localised thermal event (e.g., due to hydrothermal fluids). Lower panel: this shows how it is possible to obtain an incorrect *P-t* path if the timing of a retrograde overprint $t_{2'}$ (e.g., late zircon growth or mica recrystallisation) is incorrectly identified. **d** Schematic cross sections illustrating possible mechanisms for UHP exhumation related to: (i) divergence between the upper plate and the subducting slab leading to rapid rock exhumation within the forearc; erosional exhumation plays a minor role during exhumation. FT ages close to the timing of amphibolite facies retrogression and peak eclogite-facies conditions are predicted. (ii) Syn-convergent exhumation where erosional processes play a significant role in the exhumation of rocks within the forearc. FT ages are less than the timing of amphibolite facies retrogression and peak eclogite-facies conditions. (iii) Exhumation mechanisms are undetermined for cases in which FT ages are significantly younger than isotopic ages associated with (U)HP metamorphism

2015). An AFT age of 0.6 ± 0.2 Ma (2σ) was obtained from the coesite locality (Baldwin et al. 1993) and provides constraints on the lowest temperature portions of the *P-T-t-D* path. In general, AFT ages are challenging to obtain in these rocks, due to low apatite abundances in some rock types, low [U], and a few tracks. In eastern PNG, confined tracks are very rare, but have been imaged using heavy ion implantation to provide etchant pathways (see Chap. 2; Kohn et al. 2018). AFT ages are often close to zero, with high errors and a few track-length distributions to model, but the data are geologically meaningful and interpretable (Fitzgerald et al. 2015). Depth estimates based on preservation of coesite, together with the timing of UHP metamorphism and AFT data, indicate that average minimum exhumation rates are >1 cm/year (Baldwin et al. 1993, 2004, 2008; Hill and Baldwin 1993; Monteleone et al. 2007). (U)HP exhumation models for eastern PNG remain a topic of debate (e.g., Ellis et al. 2011; Petersen and Buck 2015), but final exposure of (U)HP rocks at the surface was likely facilitated by microplate rotation (Webb et al. 2008) and consequent divergence between the oceanic upper plate and the subducting slab (Fig. 13.2d). This kinematic scenario would have favoured the rise, from >90 km depths, of buoyant, low density, migmatitic gneisses containing mafic eclogite, via ductile flow within the subduction channel (Malusà et al. 2015, Liao et al. 2018).

The role of FT thermochronology in understanding the mechanisms of (U)HP rock exhumation is even more important in the case of the Western Alps, where (U)HP rocks have resided at shallow crustal levels during the past 30 Myr. The Western Alps formed as a result of Cretaceous to Paleogene subduction of the Tethyan oceanic lithosphere and of the adjoining European continental margin beneath the Adriatic microplate (Lardeaux et al. 2006; Zhao et al. 2015). UHP rocks are now exposed in a 20–25 km wide metamorphic belt that includes eclogitised continental crust (e.g., the Dora-Maira unit; Chopin et al. 1991) and metaophiolites (e.g., Frezzotti et al. 2011). The exhumation paths of these units are well constrained by petrologic and thermochronologic data (see Malusà et al. 2011 for a synthesis). Peak metamorphism at $P$ = 2.8–3.5 GPa and $T$ = 700–750 °C (e.g., Schertl et al. 1991; Compagnoni et al. 1995) is dated to 40–35 Ma using U–Pb ion probe analyses on zircon rims and titanite, and Sm–Nd isochron analyses (e.g., Gebauer et al. 1997; Rubatto et al. 1998; Amato et al. 1999; Rubatto and Hermann 2001). Subsequent exhumation took place at rates faster than subduction rates (Malusà et al. 2015) (Fig. 13.2b). Apatite FT and (U–Th)/He (AHe) data (e.g., Malusà et al. 2005; Beucher et al. 2012) provide constraints on the final part of the (U)HP exhumation path, attesting to rapid exhumation close to the surface by the early Oligocene, as confirmed by the biostratigraphic age of sedimentary rocks locally overlying the Western Alps eclogites (Vannucci et al. 1997).

The Western Alps example, like eastern PNG, thus illustrates the short duration between the timing of peak (U)HP metamorphism and subsequent exhumation to the Earth's surface. In this case, exhumation also occurred during the same subduction cycle that produced the (U)HP rocks, likely a result of divergent motion between the Adriatic upper plate and the European slab (Malusà et al. 2011; Solarino et al. 2018; Liao et al. 2018, Fig. 13.2d). In contrast, the Lepontine dome of the Central Alps records slower crustal exhumation (Brouwer et al. 2004; Nagel 2008), similar to the exhumational record provided by the Tso Morari eclogites in the Himalaya (de Sigoyer et al. 2000; Schlup et al. 2003). The exhumation path of the Lepontine dome is consistent with predictions of syn-convergent exhumation numerical models (e.g., Yamato et al. 2008; Jamieson and Beaumont 2013). The integration of thermochronologic and petrologic data sets thus reveals along-strike differences in exhumation patterns and mechanisms preserved in the Alpine orogenic rock record.

### 13.3.2 Pre-Cenozoic (U)HP Terranes

In the case of pre-Cenozoic (U)HP terranes such as the Dabie–Sulu of eastern China (e.g., Liou et al. 2009), the Maksyutov Massif of Russia (e.g., Lennykh et al. 1995), and the Western Gneiss (U)HP terrane of Norway (e.g., Carswell et al. 2003), FT data are even more essential to distinguish the timing and mechanisms of exhumation. This is because FT data permit assessment of whether or not final exhumation occurred during the same subduction cycle that produced the (U)HP rocks (e.g., Rohrman et al. 1995; Leech and Stockli 2000; Reiners et al. 2003; Hu et al. 2006; Kzienzyk et al. 2014). In the Western Gneiss (U)HP terrane, geochronologic data (Lu–Hf, Sm–Nd, Rb–Sr, U–Pb) have been interpreted to date the timing of (U)HP metamorphism ~430–400 Ma (Carswell et al. 2003; DesOrmeau et al. 2015). Together with thermobarometric constraints, a two-stage exhumation history for the Norwegian (U)HP terrane has been proposed. Initial exhumation, from mantle depths to lower crustal depths, was followed by stalling of the terrane at depths where mineral assemblages were overprinted during high-temperature amphibolite facies metamorphism (Walsh and Hacker 2004). Extensional processes are inferred to have led to the final exhumation to the surface. Presently, the Western Gneiss terrane is an elevated passive margin (see Chap. 20, Wildman et al. 2018). By quantifying contributions from crustal isostasy and dynamic

topography to the present-day topography, Pedersen et al. (2016) propose that high topography existed since the Caledonian orogeny (i.e., ~490–390 Ma). However, there are regional variations in Jurassic to Cretaceous AFT ages that vary as a function of elevation (Rohrman et al. 1995). Such long durations, between the timing of UHP metamorphism and ages recorded by AFT, indicate that final exhumation is not related to the same subduction cycle that formed the Western Gneiss terrane (Fig. 13.2b). Without better certainty regarding linkages between the higher and lower pressure segments of rock exhumation paths, the mechanism responsible for UHP exhumation during, or shortly after, the Caledonian subduction cycle still remains largely unconstrained.

In the Dabie–Sulu (U)HP terrane, petrologic and thermochronologic studies reveal that Triassic–Jurassic UHP metamorphism was followed by Cretaceous plutonism (Hacker et al. 1998, 2000; Ratschbacher et al. 2000). Low-temperature thermochronologic data (i.e., $^{40}Ar/^{39}Ar$ K-feldspar, AFT, (U–Th)/He on zircon (ZHe), and apatite) yielded a range of ages spanning more than 115 Myr. These data were interpreted to result from slow cooling and used to infer steady-state exhumation rates (0.05–0.07 km/Myr) (Reiners et al. 2003). Liu et al. (2017) further detail the complex thermal histories of the Sulu (U)HP terrane and report AFT and AHe ages as young as 65–40 Ma. As in the Western Gneiss Region, the long duration between UHP metamorphism and final cooling of these terranes indicates that final exhumation was not related to the subduction event that formed the Dabie–Sulu UHP terrane.

A comparison of *P-T-t* paths for selected (U)HP terranes (Fig. 13.2b) suggests that similar exhumation rates from mantle depths can be inferred, based on slopes of depth–time plots to crustal levels. The low-temperature histories of (U)HP rocks revealed by FT thermochronology can be used to distinguish between tectonic and erosional exhumation mechanisms in the upper crust (Fig. 13.2d). We caution, however, that if thermochronologic data linking segments of *P-T-t* paths from mid-crustal to shallow crustal depths are misinterpreted (e.g., based on incorrect assumptions about the pressure/inferred depth of mineral crystallisation), exhumation rates may be overestimated (segment $t_2 - t_3$ in Fig. 13.2c). For example, if $^{40}Ar/^{39}Ar$ white mica ages are interpreted as "cooling ages" (i.e., $t_2$ in Fig. 13.2c), when in fact white mica crystallised below its $T_c$ for argon, (i.e., $t_{2'}$ in Fig. 13.2c), estimated exhumation rates following mica (re)crystallisation will be incorrect. Such complications are more likely in older (U)HP terranes that have experienced a protracted evolution, with the potential for hydrothermal alteration in the upper crust.

## 13.4 Application of FT Thermochronology to Extensional Orogens: The Transantarctic Mountains

Plutonic and metamorphic rocks may preserve a record of deep orogenic processes hundreds of millions of years prior to their final exhumation to the surface. Therefore, information provided by classic petrologic and geochronologic approaches while pertinent to an earlier orogenic event may not be relevant to understanding late-stage mountain-building events and landscape evolution. The Transantarctic Mountains (TAM) case study provides an example of a protracted crustal evolution characterised by slow cooling, followed by episodic exhumation associated with rift flank formation during extensional orogenesis. The ~3500-km-long TAM mark the physiographic and lithospheric divide between East and West Antarctica (Dalziel 1992; Fig. 13.3a). The mountain belt bisects the continent and is ~100–200 km wide, with elevations locally exceeding 4500 m. The TAM define the western edge of the Mesozoic–Cenozoic intracontinental West Antarctic Rift System and the eastern margin of the East Antarctic craton, thereby providing a geomorphic barrier for the East Antarctic Ice Sheet. The TAM are related to formation of the West Antarctic rift and are inferred to represent an erosional remnant of a collapsed plateau (Bialas et al. 2007), with the rift flank associated with flexure of strong East Antarctic lithosphere (e.g., Stern and ten Brink 1989).

The overall geology of the TAM is relatively simple (e.g., Elliot 1975). Basement rocks are composed primarily of Late Proterozoic–Cambrian metamorphic rocks and Cambrian–Ordovician granitoids of the Granite Harbour Intrusive Suite (Fig. 13.3a). Basement rocks were deformed during the Cambrian–Ordovician Ross Orogeny that preceded and accompanied intrusion of granitoids (e.g., Goodge 2007). Following the Ross Orogeny, 16–20 km of rock exhumation resulted in formation of the low-relief Kukri Erosion Surface (Gunn and Warren 1962; Capponi et al. 1990). Basement rocks were subsequently unconformably overlain by Devonian–Triassic glacial, alluvial, and shallow marine sediments of the Beacon Supergroup (e.g., Barrett 1991). During the Jurassic, extensive basaltic magmatism (Ferrar large igneous province) occurred along the TAM, as well as in adjoining parts of Gondwana, South Africa, South America, and southern Australia (e.g., Elliot 1992; Elliot and Fleming 2004). Dolerite sills (up to 300 m thick) intruded both basement and sedimentary cover. Step heat experiments on feldspars from the sills yielded $^{40}Ar/^{39}Ar$ ages of 177 Ma (Heimann et al. 1994). Mafic volcanism (i.e., the Kirkpatrick Basalt; Elliot 1992) was contemporaneous with dolerite sill

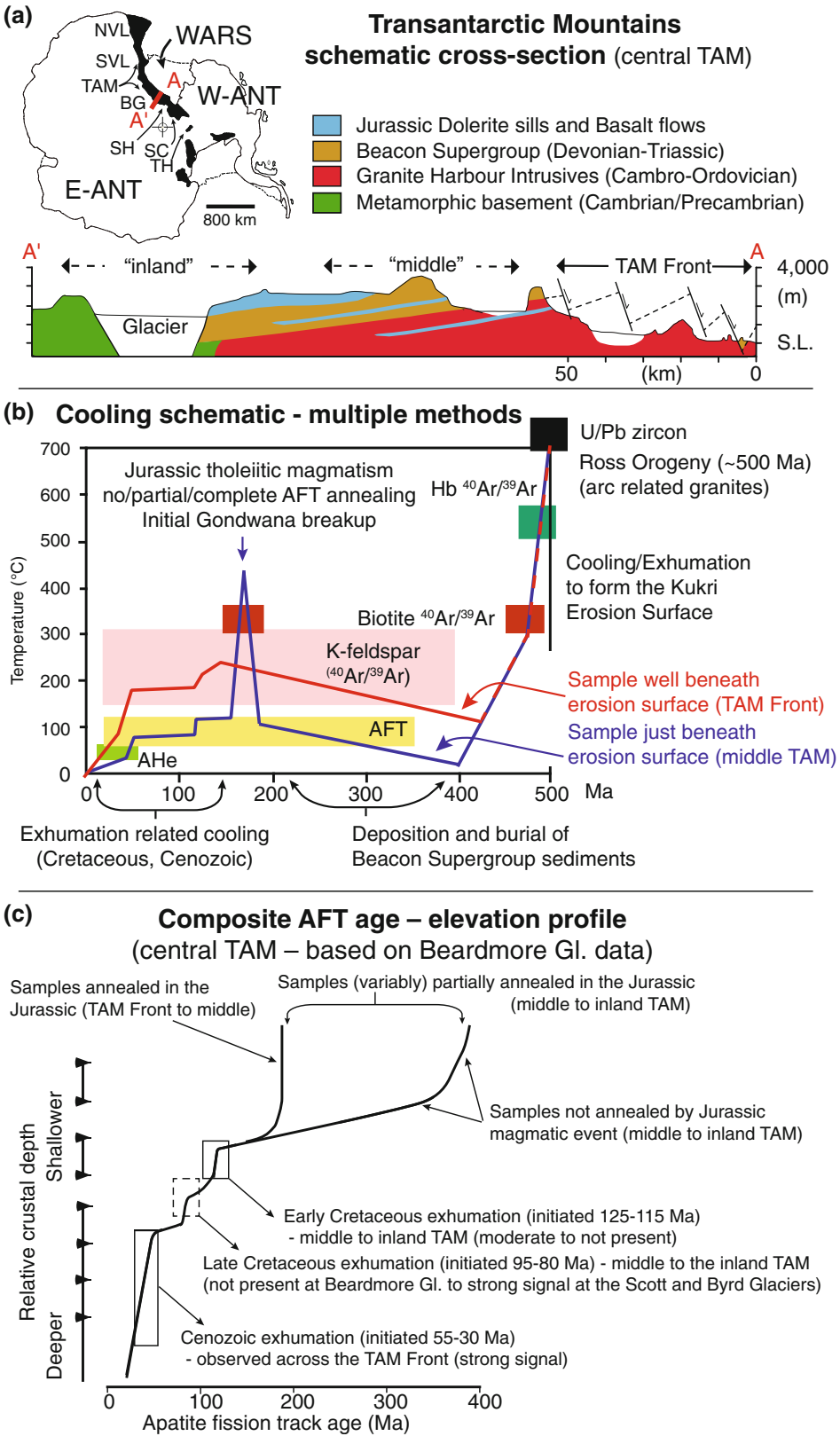


**Fig. 13.3** **a** Map of Antarctica and schematic cross section (A-A′) of the TAM in the Shackleton–Beardmore–Byrd glacier region showing simplified geology. Shallowly dipping rocks of the TAM extend beneath the East Antarctic Ice Sheet. Normal faults in the TAM front expose more deeply exhumed plutonic rocks of the Cambrian–Ordovician Granite Harbour Intrusives (modified after Barrett and Elliot 1973; Lindsay et al. 1973; Fitzgerald 1994). Black regions are TAM with approximate locations indicated: BG = Beardmore Glacier, NVL and SVL = northern and southern Victoria Land, SC = Scott Glacier, SH = Shackleton Glacier, TH = Thiel Mountains. **b** Schematic composite temperature–time plot for samples below the Kukri Erosion Surface (purple) and from the TAM front (i.e., at deeper crustal levels; red). **c** Composite AFT age—crustal depth profiles for the central TAM, Beardmore glacier region illustrating differential cooling, and exhumation patterns revealed by AFT ages. After Fitzgerald (1994), Fitzgerald and Stump (1997), and Blythe et al. (2011) for the Byrd Glacier

emplacement. The present-day outcrop pattern of the TAM generally reflects its simple tilt block structure dipping inland (Fig. 13.3a). Outcrops of Kirkpatrick Basalt are limited to the inland parts of the range, whereas basement representing deeper crustal levels is exposed primarily along the coastal sector, extending inland along major outlet glaciers. In a few coastal locations such as Cape Surprise in the central TAM (Barrett 1965; Miller et al. 2010), Beacon Supergroup rocks are down-faulted by 3–5 km. Beacon Supergroup rocks have also been recovered offshore southern Victoria Land at a depth of 825 m below seafloor in the Cape Roberts drillhole#3 (Cape Roberts Science Team 2000). In most cases, AFT ages on basement rocks were (i) completely reset as a result of the thermal effects of Jurassic magmatism (Fig. 13.3b) or (ii) were resident at depths below the base of the PAZ prior to Cretaceous and younger exhumation (e.g., Gleadow and Fitzgerald 1987). However, along the inland flank of the TAM, un-reset or partially reset AFT ages (Fig. 13.3c) have been documented (Fitzgerald and Gleadow 1988; Fitzgerald 1994).

Following Jurassic tholeiitic magmatism, and prior to Late Cenozoic alkaline volcanism of the McMurdo Volcanic Group (LeMasurier and Thomson 1990), a ~160 Myr gap in the onshore geologic record of the TAM exists. Coring of sedimentary basins in the Ross Sea recovered sediment as old as Upper Eocene (Barrett 1996; Cape Roberts Science Team 2000). However, because no core older than Upper Eocene has been recovered from adjacent sedimentary basins, and the onshore geologic record is missing, studies of the uplift and exhumation history of the TAM have relied primarily on the application of thermochronology, largely AFT thermochronology on basement granitoids (e.g., Gleadow and Fitzgerald 1987). More recently, detrital thermochronology on drill core from the West Antarctic rift provides additional contributions to our understanding of the TAM exhumation history (e.g., Zattin et al. 2012).

### 13.4.1 Sampling Strategy, Data, and Interpretation

The TAM front (Barrett 1979) is marked by a major normal fault zone, extending ~20–30 km inland from the coast and resulting in 2–5 km of displacement down to the coast (Fitzgerald 2002). The amount of exhumation decreases inland as inferred from the geological outcrop pattern and overall architecture of the TAM (Fig. 13.3a). The level of exhumation, combined with spectacular outcrops of Ross Orogen granites, often rich in accessory minerals, means that AFT has proven to be the best method to constrain the exhumation history of the TAM (Fig. 13.3b). The sampling strategy involved collecting granitic samples over significant relief across the range. AFT data revealed multiple exhumed PAZs, defined by breaks in slope (see Chap. 9, Fitzgerald and Malusà 2018) in age–elevation profiles across the mountains. These data were interpreted to indicate periods of exhumation separated by periods of relative thermal and tectonic stability, i.e., episodic exhumation (Gleadow and Fitzgerald 1987; Fitzgerald and Gleadow 1990; Stump and Fitzgerald 1992). Samples above the break in slope contain shorter confined mean track lengths with larger standard deviations, a result of prolonged durations spent in the PAZ where track lengths are partially annealed (i.e., shortened). As the amount of exhumation decreases inland across the TAM (and the elevation of the range increases), AFT ages become older. The timing of the breaks in slope, representing the base of exhumed PAZs, also becomes older inland as the amount of exhumation decreases. These data reveal the timing, amount, and rate of rock exhumation in the TAM (e.g., Gleadow and Fitzgerald 1987; Fitzgerald and Gleadow 1990; Fitzgerald, 1992, 1994, 2002; Stump and Fitzgerald 1992; Balestrieri et al. 1994, 1997; Gleadow et al. 1984; Fitzgerald and Stump 1997; Lisker 2002; Miller et al. 2010). Exhumation rates, determined from the slope of age–elevation profiles below the break in slope, indicate rates typically <200 m/Myr. Because exhumation is so slow, heat is transported primarily via conduction, and advection has not modified the slope of the profile (e.g., Brown and Summerfield 1997). While there are many caveats to take into account when using the slope of an age–elevation profile to constrain the exhumation rate (e.g., Braun 2002, see also Chap. 9, Fitzgerald and Malusà 2018), corrections for topographic effects in the TAM are likely to be minimal (e.g., Fitzgerald et al. 2006).

The age trends and exhumation history are dependent on the location of a sample (or age profile) along the TAM, as well as its location across the range (Fig. 13.3c). Late Jurassic exhumation revealed in the Thiel Mountains, and well inland of the present-day rift flank (Fitzgerald and Baldwin 2007) is in general followed by periods of Early and Late Cretaceous exhumation. The major period of exhumation accompanying rock uplift that formed the TAM began in the Early Cenozoic (Gleadow and Fitzgerald 1987; Fitzgerald and Gleadow 1988; Fitzgerald 1992, 2002), but periods of more rapid exhumation in the Oligocene and Early Miocene have also been documented. The onset of early Cenozoic exhumation is variable along the TAM, younging from north to south: ~55 Ma in northern Victoria Land and southern Victoria Land, ~50 Ma in the Beardmore Glacier area and the Shackleton Glacier, and ~45 Ma in the Scott Glacier region. In places, an inland-younging trend of AFT ages is also apparent (e.g., in the Shackleton Glacier; Miller et al. 2010; in southern Victoria Land; Fitzgerald 2002). This inland-younging trend is interpreted to result from escarpment retreat at a rate of ~2 km/Myr, with the retreat rate apparently slowing

dramatically ~10 Myr following onset of early Cenozoic exhumation (Miller et al. 2010). Exhumation rates also vary across the TAM, decreasing inland as the overall amount of rock uplift decreases.

### 13.4.2 Comparison with Other Thermochronologic Data Sets, and Tectonic Implications

Application of multiple thermochronologic methods on cogenetic minerals has confirmed that AFT data and inverse thermal models, on samples collected over varying elevations, provide the most information on the formation of the TAM. For example, $^{40}Ar/^{39}Ar$ data on K-feldspars from the Thiel Mountains (Fitzgerald and Baldwin 2007) yield Paleozoic ages which are significantly younger than granitoid crystallisation ages (Fig. 13.3b). The $^{40}Ar/^{39}Ar$ K-feldspar data are interpreted to date the timing of cooling associated with erosional exhumation that led to the formation of the Kukri Erosion Surface. In the Ferrar Glacier region of southern Victoria Land, AHe single grain ages on an age–elevation profile collected in granitic rocks yielded considerable intrasample variation that could be correlated with cooling rate, but in combination with AFT data indicated episodes of exhumation in the Cretaceous and Eocene (Fitzgerald et al. 2006). Detrital geochronology from glacial deposits yields Paleozoic and Mesozoic ages, with variable ZHe (480–70 Ma) and AHe (200–70 Ma) ages (Welke et al. 2016). Detrital data from drillholes offshore southern Victoria Land (Zattin et al. 2012; Olivetti et al. 2013) support the onshore AFT interpretations but also add information about provenance and younger exhumation events to the south along the TAM.

To summarise, AFT thermochronology successfully reveals the timing and patterns of Late Jurassic, Early Cretaceous, Late Cretaceous, and Cenozoic exhumation events in the TAM. These studies confirmed that erosional exhumation that formed the Kukri peneplain was not the mechanism responsible for the formation and landscape evolution of the TAM. Instead, episodic exhumation can be related to regional tectonic events including:

- Jurassic rifting and accompanying widespread basaltic magmatism (Ferrar large igneous province) that variably reset AFT ages;
- Plateau collapse and the initial break-up between Australia and Antarctica in the Early Cretaceous;
- Extension between East and West Antarctica in the Late Cretaceous accommodated on low-angle extensional faults (in the Ross Embayment and Marie Byrd Land);
- Southwards propagation of a seafloor spreading rift tip, from the Adare Trough into continental crust underlying the western Ross Sea in the Early Cenozoic (e.g., Fitzgerald and Baldwin 1997; Fitzgerald 2002; Bialas et al. 2007).

## 13.5 Application of FT Thermochronology to Compressional Orogens: The Pyrenees

Thermal histories of plutonic and metamorphic rocks inferred from compressional orogens are often complicated (e.g., Dunlap et al. 1995; ter Voorde et al. 2004; Lock and Willett al. 2008; Metcalf et al. 2009). This is because thrusting does not exhume rocks, thrust burial may reset or partially reset thermochronologic systems, and rocks may undergo multiple periods of cooling and exhumation. Thrusting may also be in-sequence or out-of-sequence. Thus, a full understanding of the geologic and structural evolution is usually required before optimal sampling strategies can be developed. In this case study of the central Pyrenees, we illustrate how integration and modelling of thermochronologic data on cogenetic minerals from plutonic rocks collected in vertical profiles reveal a geologic evolution spanning 300 Myr. The results are interpreted with respect to magma crystallisation and cooling, exhumation, burial, heating during thrusting, burial and final exhumation (re-excavation) to the surface.

The Pyrenees mountains began to form in the Late Cretaceous as a result of convergence between the European and Iberian plates (Fig. 13.4a) (e.g., Munoz 2002). The core of the range (i.e., the Axial Zone) consists of an antiformal south-vergent duplex structure, composed of imbricate thrust sheets of Hercynian basement (Fig. 13.4b). The Axial Zone is flanked to the north and south by fold-and-thrust belts. Prior to the onset of convergence in the Late Cretaceous, the region now occupied by the Pyrenean mountain range was the site of Triassic and Early Cretaceous rift basins (e.g., Puigdefabregas and Souquet 1986). During the Late Cretaceous, some of the rift basins and much of the Axial Zone were below sea level, as indicated by Upper Cenomanian shallow-water carbonates that grade into deeper marine sediments and turbidites north of the Axial Zone (Seguret 1972; Berastegui et al. 1990). In the Maastrichtian, the foreland basins shallowed to tidal conditions and received continental fluvial sediments sourced by basement rocks. Initial convergence and crustal thickening were accommodated prior to the development of significant topography above sea level (McClay et al. 2004). Deformation within the orogen proceeded from north to south such that thrust sheets or portions of a thrust sheet (footwall, hanging wall, proximal to the fault, distal to the fault) preserve different aspects of the Pyrenean orogenesis. Exhumation in the Pyrenees is dominantly erosional (e.g., Morris et al. 1998);

thus, age patterns determined from low-temperature thermochronology (e.g., AFT and AHe) are usually interpreted with respect to the emergence and erosion of topography, and/or changes in base level following thrusting. Late Paleozoic biotite $^{40}Ar/^{39}Ar$ ages (Fig. 13.4c) document the timing of crystallisation of Hercynian intrusives, with variable degrees of partial resetting interpreted to result from Pyrenean orogenesis (e.g., Jolivet et al. 2007). $^{40}Ar/^{39}Ar$ K-feldspar age spectra were interpreted to result from argon loss via volume diffusion due to thrust burial and heating. Therefore, it is the low-temperature thermochronologic methods that document the timing and duration of thrusting, burial, and exhumation during intracontinental convergence.

### 13.5.1 Multi-method Thermochronology on Cogenetic Minerals from Vertical Profiles

In developing a sampling strategy, it is important to first recognise that the thermal evolution of footwall and hanging wall rocks within imbricate thrust sheets (e.g., the antiformal south-vergent duplex structure in the Pyrenees) varies as a function of position within the thrust system (ter Voorde et al. 2004; Metcalf et al. 2009). As intracontinental convergence proceeds, rocks at different structural positions will preserve a record of different maximum and minimum temperatures during burial due to thrust loading. The thermal history revealed by thermochronologic analysis of minerals will therefore vary with structural position (Fig. 13.4b). As long as displacement rates are sufficiently slow to allow for conductive thermal equilibration (e.g., Husson and Moretti 2002), the timing and relative magnitude of thermal events should agree. However, the maximum and minimum temperatures recorded by low-temperature thermochronologic methods will vary systematically, dependent upon the sample's structural position.

Here, we use a thermochronologic study of cogenetic minerals from granitoid samples, collected over ~1450 m relief within the Maladeta Pluton of the Pyrenean Axial Zone, to illustrate how application of AFT, AHe, and $^{40}Ar/^{39}Ar$ methods reveals the burial and exhumation history during thrusting and nappe emplacement (Metcalf et al. 2009). The Maladeta Massif lies within the Orri thrust sheet, presently occupying the immediate footwall of the Gavarnie Thrust, a major Alpine-age thrust fault (Fig. 13.4b). Biotite and K-feldspar from the highest elevations of the Maladeta Pluton (2850 m) in the central Axial Zone yielded maximum $^{40}Ar/^{39}Ar$ ages of ~280 Ma, close to the age of intrusion and interpreted to date the timing of rapid cooling during the Hercynian orogeny (Fig. 13.4c). All $^{40}Ar/^{39}Ar$ step heat experiments on K-feldspars yielded disturbed age spectra (i.e., age gradients), with the degree of partial $^{40}Ar^*$ loss varying as a function of sample elevation, and consistent with each sample's structural position in the footwall of the Gavarnie Thrust (Metcalf et al. 2009). Thus, the highest elevation sample experienced the least amount of $^{40}Ar^*$ partial loss, while the lowest elevation sample experienced the greatest amount of $^{40}Ar^*$ loss. Minimum $^{40}Ar/^{39}Ar$ K-feldspar ages associated with each age spectrum were interpreted to result from argon loss via volume diffusion due to thrust burial and heating.

AFT thermochronology on samples from the Maladeta profile (Fig. 13.4d) yielded ages and track-length distributions that varied as a function of elevation (Fitzgerald et al. 1999). The upper part of the profile (i.e., samples at highest elevations; 1945–2850 m) gave concordant AFT ages, with mean track lengths $\geq$14 μm for confined track-length distributions. Data from this part of the Maladeta profile were interpreted to result from rapid cooling due to exhumation between ~35 and ~32 Ma at rates of 1–3 km/Myr. The lower part of the profile (i.e., samples at 1125–1780 m elevations) yielded younger AFT ages that decrease with decreasing elevation. These samples were interpreted as reflecting slower exhumation and partial annealing due to burial of the southern flank of the Pyrenees by syn-tectonic conglomerates shed off the eroding Axial Zone thrust sheets (Coney et al. 1996). The form of the lower part of the age–elevation profile when interpreted within the geologic framework implies that there must have been Late Miocene re-excavation of the syn-tectonic conglomerates that filled the foreland basin and that were overlying the fold-and-thrust belt. Fillon and van der Beek (2012) undertook thermo-kinematic modelling to evaluate various tectonic and geomorphic scenarios using this AFT data as well as AHe ages from this region (Gibson et al. 2007; Metcalf et al. 2009). Their best-fit models, started at 40 Ma, indicated there was rapid exhumation between ~37 and 30 Ma at rates of >2.5 km/Myr followed by infilling of topography by syn-tectonic conglomerates with re-excavation and incision of the southern Pyrenean wedge beginning ~9 Ma.

While AFT and AHe thermochronology are discussed above constrain thermal histories from ~120 to ~40 °C, K-feldspar $^{40}Ar/^{39}Ar$ data and multi-diffusion domain (MDD) models extend the thermal histories into the higher temperature range of 350–150 °C (Lovera et al. 1989, 1997, 2002). Assuming that argon retention in nature and argon loss in the laboratory are controlled by thermally activated volume diffusion, argon data from step heat experiments can be inverted to yield continuous cooling histories (Lovera et al. 2002). Although K-feldspars from the Maladeta Pluton have experienced a complex geologic history, MDD models of $^{40}Ar/^{39}Ar$ K-feldspar data yielded continuous *T-t* histories between the higher and lower temperature thermochronologic constraints. The combined K-feldspar MDD, AFT, and AHe best-fit thermal models for each sample form

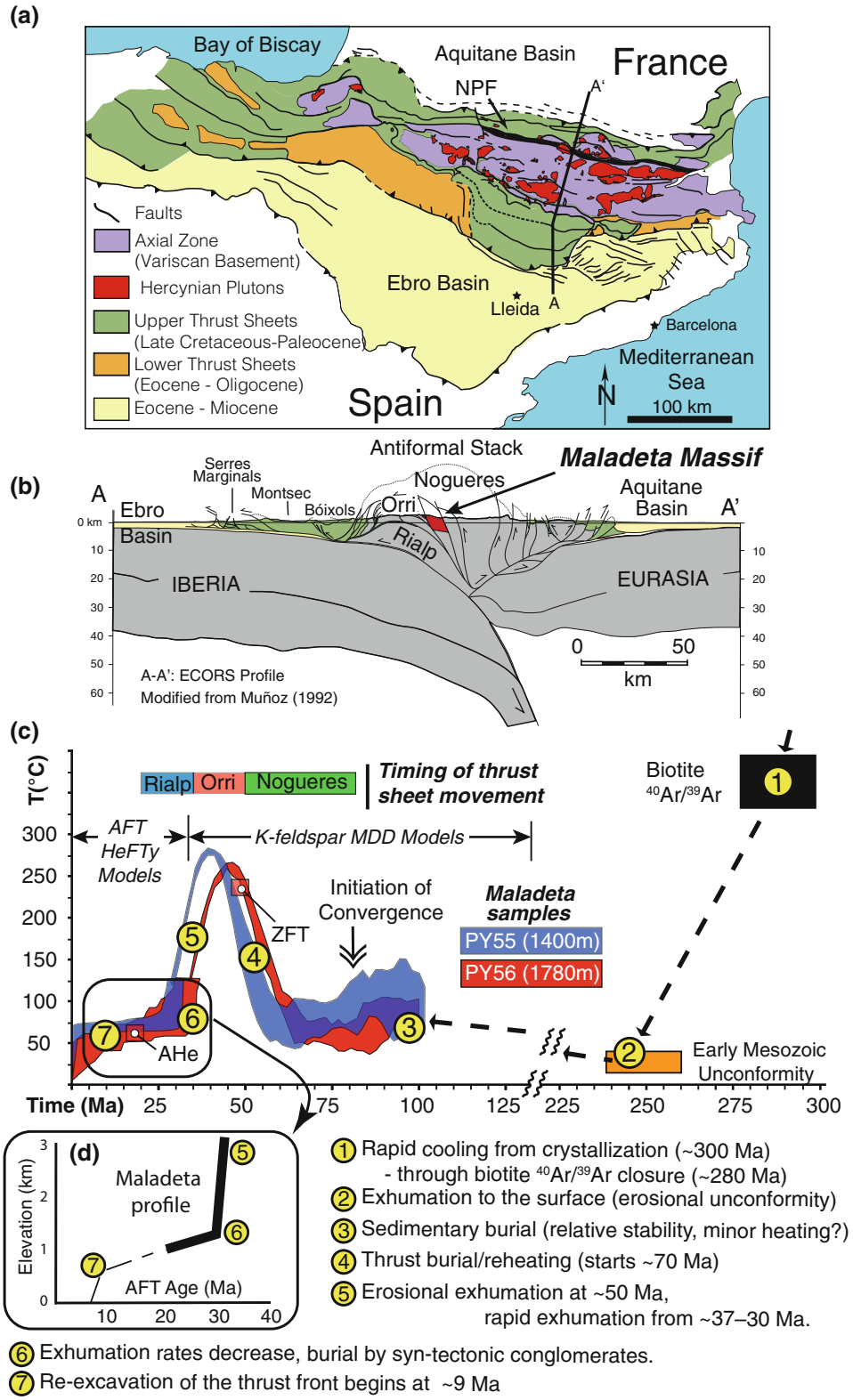


**Fig. 13.4** **a** Simplified geologic map of the Pyrenean orogen with **b** ECORS cross section (A-A′) indicated (modified from Fitzgerald et al. 1999; Munoz 2002; Verges et al. 2002; Metcalf et al. 2009). **c** Compilation of the thermal constraints for the Maladeta Pluton (modified from Metcalf et al. 2009, with additional information from Fillon and van der Beek 2012). **d** Simplified AFT age—elevation profile from the Maladeta Massif (modified from Fitzgerald et al. 1999, with additional information from Fillon and van der Beek 2012)

overlapping thermal history "dovetails" (e.g., PY55 and PY56; Metcalf et al. 2009; Fig. 13.4c) that are interpreted to date the timing of imbricate thrusting to form the Axial Zone antiformal stack. Ages and models obtained using different techniques are both internally consistent and most importantly agree with all available geologic observations. For example, the onset of heating and maximum temperatures, as indicated by thermal models, correlate with structural position and lateral distance from the Gavarnie Thrust and are also consistent with the geologic history of progressive burial of the Maladeta Pluton under a south-vergent thrust sheet (Munoz 2002).

### 13.5.2 Tectonic Interpretation and Methodologic Implications

We can summarise the thermochronologic data from the Maladeta Pluton and integrate it with geologic constraints to determine evolution of the pluton spanning 300 Myr. The thermal and geologic history includes magma crystallisation and cooling during the Hercynian orogeny, followed by cooling and exhumation to the surface. Mesozoic sediment deposition led to burial of plutonic rocks. Convergence of Iberia with Europe during the Alpine orogeny led to thrusting, heating due to overthrusting, exhumation to the surface in a number of phases, reburial by syn-tectonic conglomerates, and then final re-excavation in the Late Miocene (Fig. 13.4c, d). Following magma crystallisation at ~300 Ma, initial cooling to below ~325–400 °C is recorded by ~280 Ma biotite $^{40}Ar/^{39}Ar$ ages (Metcalf et al. 2009). Subsequent cooling, as plutonic rocks were exhumed to the surface, is constrained in part by the Late Paleozoic–Early Mesozoic erosional unconformity preserved in the northern Maladeta Pluton (Zwart 1979). During the Mesozoic, plutonic rocks remained largely below sea level as shallow marine sediments were deposited. Burial and heating of the Maladeta Pluton in the footwall of the Gavarnie Thrust are recorded in both K-feldspar $^{40}Ar/^{39}Ar$ data and MDD thermal models, as well as reset Cenozoic AFT ages in a region that was at the surface in the Late Paleozoic–Early Mesozoic (Munoz 1992). The onset of erosional exhumation in the Maladeta at ~50 Ma is recorded by K-feldspar $^{40}Ar/^{39}Ar$ MDD thermal models with accelerated exhumation from 37 to 30 Ma confirmed by AFT age–elevation relationships and modelling (Fitzgerald et al. 1999; Metcalf et al. 2009; Fillon and van der Beek 2012). From ~30 Ma to the present, a decrease in exhumation rate is recorded by AFT thermal models and age–elevation relationships for both AFT and AHe data, with subsequent re-excavation of the southern flank of the Pyrenees beginning at ~9 Ma. No single mineral/method reveals the complete thermal history that can be interpreted with respect to the timing and duration of thrusting, burial, and exhumation during intracontinental convergence. In this case, AFT and AHe data from both the hanging wall and footwall of the Gavarnie Thrust only provide minimum age constraints on thrust fault activity and underestimate the onset of thrust fault activity by as much as 30 Myr. The complex thermal histories revealed by multi-method thermochronology on cogenetic minerals from vertical (age–elevation) profiles also illustrate that mineral ages from these plutonic samples cannot be simply interpreted with respect to bulk closure temperatures. This Pyrenean example illustrates the necessity of combining multiple techniques as well as thermal modelling to fully reveal and interpret the geodynamic evolution of intracontinental convergent orogens.

## 13.6 Application of FT Thermochronology to Transpressional Plate Boundary Zones: The Alpine Fault of New Zealand

Continental transform plate boundary zones are characterised by dominantly highly localised strike-slip shear zones. Their orientation changes as they evolve, and in cases where plate motion has a significant oblique component, spectacular mountain ranges may form. In this case study, we highlight how FT thermochronology has been used to document the geodynamic evolution of the plate boundary zone in the South Island of New Zealand. The interpretation of thermochronologic data in this rapidly evolving dynamic plate boundary is complicated due to heat advection and potential (re)crystallisation associated with fluid–rock interaction. As new data (i.e., temperature, fluid pressure) from active plate-bounding faults are obtained (Sutherland et al. 2017), FT data interpretations may require re-evaluation, particularly in cases where there is evidence for late-stage fluids that transport heat and may have caused (partial) annealing of fission tracks.

### 13.6.1 Tectonic and Geologic Setting

The South Island of New Zealand straddles the Australian-Pacific plate boundary zone and is actively undergoing oblique continent–continent convergence (e.g., Walcott 1998). In the North Island and north-eastern part of the South Island, oceanic crust of the Pacific (PAC) plate subducts westwards beneath the Australian (AUS) plate. In the south western most part of the South Island, subduction polarity reverses, and the AUS plate subducts eastwards beneath the PAC plate. Both subduction systems are linked by a wide, dextrally transpressional fault zone in the South Island that has evolved since the latest Oligocene to Early Miocene (e.g., Cox and Sutherland 2007) with the Alpine

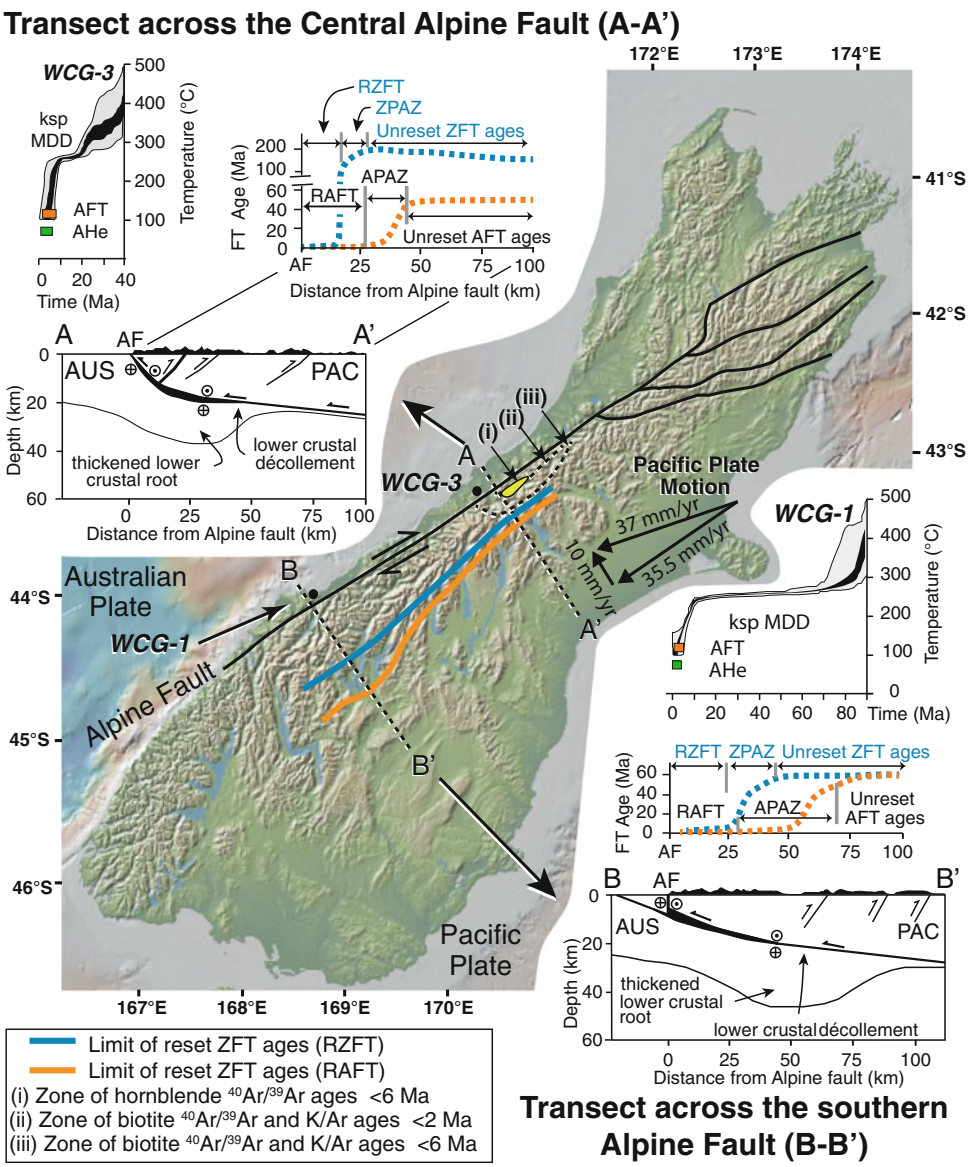


**Fig. 13.5** Digital elevation model of the AUS-PAC transpressional plate boundary zone in the South Island of New Zealand made using GeoMap app (http://www.geomapapp.org; Ryan et al. 2009). Cross sections of the central portion of the Southern Alps (A-A′) and southern segment of the Southern Alps (B-B′) after Warren-Smith et al. (2016). Nested regions of reset $^{40}Ar/^{39}Ar$ hornblende ages (*i* (in yellow)), and biotite ages (*ii* (dashed), and *iii* (dashed)); after Little et al. 2005), and plots of AFT and ZFT ages versus distance from the Alpine Fault after Warren-Smith et al. 2016 and Tippett and Kamp 1993). Time–temperature envelopes derived from MDD models of K-feldspar $^{40}Ar/^{39}Ar$ data for samples WCG-3 and WCG-1 from West Coast granites (AUS plate affinity) from Batt et al. (2004)

fault zone marking the continental transform (Fig. 13.5). While the majority of the plate motion is accommodated on the Alpine Fault, slip is distributed and accommodated on faults across the entire South Island, as indicated by active seismicity and geodetic studies (e.g., Beavan et al. 2007; Wallace et al. 2006). Both geology and geodesy constrain the horizontal components of the displacement field, including velocities, strain and strain rates. Present-day AUS-PAC relative plate motion indicates that deformation is broadly partitioned into a strike-slip component of 33–40 mm/year and a fault-normal compressive component of 8–10 mm/year (Beavan et al. 2007). The Southern Alps, one of the fastest rising and eroding mountain ranges in the world, consists of (meta)greywacke that was progressively thickened to form a crustal monocline within the dextrally transpressive Alpine fault zone. Geodetic data for the central portion of the Southern Alps region, corresponding to the Alpine fault zone and straddling the area of highest topographic relief (i.e., the Mt. Cook region), indicate surface vertical uplift rate estimates ranging from 5 to 8 mm/year (Beavan et al. 2002, 2010; Houlie and Stern 2012), comparable to rock uplift rates and exhumation rates derived from thermochronology, as discussed below.

Basement rocks of the South Island are divided broadly into a Western Province consisting mainly of granite and gneiss of AUS plate affinity, and an Eastern Province of PAC affinity consisting primarily of metamorphosed Permian to Lower Cretaceous Torlesse greywacke and the Haast Schist Belt comprising the Otago and Alpine schists (e.g., Cox and Sutherland 2007). The transpressive AUS-PAC plate boundary zone is a relatively broad anastomosing network of high strain zones (e.g., Toy et al. 2008, 2010) in

which slivers of both hanging wall Alpine Schist (PAC affinity) and footwall Western Province rocks (AUS affinity) have been incorporated and heterogeneously deformed. Details of the early evolution of the modern orogen (i.e., the Southern Alps of PAC provenance) have yet to be fully revealed (e.g., Cox and Sutherland 2007). However, application of multiple thermochronologic methods on cogenetic K-feldspar and apatite from rocks of the Western Province (i.e., of AUS provenance located west of the Alpine Fault) has demonstrated that the early evolution of the Alpine fault zone is preserved in the footwall of the Alpine Fault (e.g., Batt et al. 2004) (Fig. 13.5, samples WCG-1 and WCG-3).

A steeply dipping metamorphic belt is exposed in the hanging wall (PAC) of the Alpine Fault where the metamorphic grade of Alpine Schist generally increases westwards towards the fault, reaching the oligoclase zone of the amphibolite facies (e.g., Cooper 1972, 1974). Temperatures and pressures reached by hanging wall greywackes were inferred assuming metamorphic assemblages achieved equilibrium (Grapes and Wattanabe 1992), corresponding to metamorphic mineral isograds (e.g., garnet, biotite; Little et al. 2005). However, metamorphic mineral(s) crystallised over a range of P-T conditions, where the availability of aqueous fluids enhanced reaction rates, triggering new mineral growth and recrystallisation of protoliths. As (re) crystallisation continued, complete to partial resetting of isotopic systematics within the minerals occurred. For example, zoned Late Cretaceous garnets have rims that overgrew the Alpine Fault mylonitic foliation (Vry et al. 2004). Fabrics preserve polyphase deformational histories in Alpine Fault mylonites (Toy et al. 2008), as indicated by porphyroclastic biotite (inherited from the Alpine Schist) and neocrystallised biotite within the mylonite zone in the hanging wall of the Alpine Fault (Toy et al. 2010).

### 13.6.2 Thermochronologic Data and Geologic Interpretation

For more than 35 years, thermochronologic studies have contributed to understanding the AUS-PAC plate boundary evolution and the landscape evolution of the Southern Alps (Fig. 13.5). Early studies documented that radiometric ages vary across the structural trend of the mountains (Sheppard et al. 1975; Adams 1980; Adams and Gabites 1985; Kamp et al. 1989; Tippett and Kamp 1993). Thermochronologic data have commonly been interpreted as ages corresponding to bulk $T_c$ (e.g., Batt et al. 2000; Little et al. 2005). In the case of more retentive thermochronologic systems (e.g., $^{40}Ar/^{39}Ar$ mineral ages), age variations have also been suggested to be a result of variable post-metamorphic cooling involving partial Ar loss during Neogene exhumation (Adams and Gabites 1985; Chamberlain et al. 1995) and/or "excess Ar" (Batt et al. 2000). FT ages from the Alpine Schist are generally interpreted to indicate the timing of Neogene cooling and exhumation (e.g., Kamp et al. 1989; Batt et al. 1999). Map compilations have been made that indicate the amount of exhumation in the Southern Alps (Tippett and Kamp 1993; Batt et al. 2000). These studies have interpreted isotopic ages as the timing of exhumation *from below the related closure depth* (i.e., the depth at which the ambient crustal temperature exceeds the respective $T_c$), assuming a "pre-uplift geothermal gradient".

Transects across the central and southern Alpine Fault (A-A′ and B-B′ in Fig. 13.5) reveal reset AFT and ZFT ages east of the Alpine Fault with the youngest ages (Middle Miocene and younger) adjacent to the Alpine Fault (e.g., Kamp et al. 1989; Tippett and Kamp 1993; Batt et al. 2000; Herman et al. 2009; Warren-Smith et al. 2016). With progressive increase in distance from the Alpine Fault (25–100 km), AFT and ZFT ages gradually increase from reset to partially annealed samples and then older (i.e., un-reset) samples, reaching Early Cenozoic and Mesozoic ages, respectively. These data have been interpreted to reflect a higher rock uplift rate and deeper exhumation closer to the Alpine Fault. The greatest amount of exhumation occurs within a narrow ~50-km-long segment centred on the Franz Josef Glacier region where the highest peaks occur. In the central portion of the Southern Alps (A-A′ in Fig. 13.5), a narrow zone of reset FT ages has been identified that coincides with where the fault is steeper, where back-thrusting has built up topography, and where erosional exhumation is enhanced. In the central portion, the lower crustal root is thinner as compared to the southern portion of the Southern Alps. In the southern segment (B-B′ in Fig. 13.5), a wider zone of reset FT ages occurs, where the fault dip is shallower, the deformation zone is wider, and strain is partitioned over a larger region.

On the AUS (western) side of the plate boundary zone, temperature–time plots compiled using MDD models based on $^{40}Ar/^{39}Ar$ K-feldspar data together with AFT and AHe data (Batt et al. 2004) are shown for central (WG-3) and southern sections (WG-1) of the Alpine fault zone (Fig. 13.5). Also indicated (close to WG-3) are regions east of the Alpine Fault where $^{40}Ar/^{39}Ar$ hornblende and biotite ages are <6 Ma (Chamberlain et al. 1995; Little et al. 2005). Despite complexity in the data, and differences in presentation of thermochronologic data sets, some comparisons can be made for these locations. For example, gneisses and granites from the AUS side of the central portion of the fault zone contain K-feldspar that resided for shorter duration within the argon PRZ as compared to K-feldspars from the AUS side of the southern segment of the fault zone (Fig. 13.5). K-feldspar from the southern segment of the AUS plate preserves more of the pre-20 Ma history.

However, considerable scatter in isotopic ages from adjacent samples using the same mineral/method has rendered interpretation challenging (e.g., Warren-Smith et al. 2016) and also calls into question simple $T_c$ interpretations and exhumation rate calculations based on assumed temperature to depth conversions. For example, Ring et al. (2017) used total fusion illite $^{40}Ar/^{39}Ar$ ages (1.36 ± 0.27 Ma, 1.18 ± 0.47 Ma), along with ZFT (0.79 ± 0.11 and 0.81 ± 0.17 Ma) and ZHe ages (0.35 ± 0.03 and 0.4 ± 0.06 Ma) from fault gouge to construct a cooling history assuming bulk $T_c$ for each mineral/method pair. However, illite from fault gouge directly above the current trace of the Alpine Fault yielded complex $^{40}Ar/^{39}Ar$ laser spectra with apparent ages, corresponding to a significant percentage of $^{39}Ar$ released, within error of zero. Alternative interpretations, invoking partial (re)crystallisation and partial loss of radiogenic daughter products, are possible.

Toy et al. (2010) argue, based on Alpine fault zone materials now exposed at the surface, that geothermal gradients in the crust above the structural brittle–viscous transition are ~40 °C/km and decrease to ~10 °C/km below the structural brittle–viscous transition. Geothermal gradients evolved over time and were locally modified due to heat advection resulting from focused fluid flow, as documented by temperature and fluid pressure data from the Alpine Fault (e.g., Sutherland et al. 2017, and references therein). The Sutherland et al. study measured an average geothermal gradient of 125 ± 55 °C/km in a borehole drilled in the hanging wall of the Alpine Fault. Such high temperatures are sufficient to reset AFTs at relatively shallow depths and indicate that the present-day AFT PAZ is at a depth of only 400–800 m at this location. Exhumation-related fluid flow has been used to explain the pairing of seismic and electrical conductivity anomalies observed in the Southern Alps in New Zealand (e.g., Jiracek et al. 2007; Stern et al. 2007), low-frequency earthquake activity (Chamberlain et al. 2014), as well as the formation of abundant vein-infilled back shears in the Alpine Schist (e.g., Wightman and Little 2007). These results provide further evidence for extensive hydration in the brittle part of the Alpine Fault, with sufficiently large fluid fluxes capable of advecting heat and elevating thermal gradients on a local scale. Advective heat flow may also trigger recrystallisation (via dissolution–reprecipitation), of thermochronologically relevant mineral phases. Apatite is susceptible to metasomatic (fluid-induced) alteration over a wide range of pressures and temperatures, and even surface conditions (Harlov et al. 2005; Harlov 2015). Zircon is also prone to diagenetic and low-temperature metamorphic growth driven by fluids, especially in radiation-damaged zones of zircon crystals (Rubatto 2017). Given sufficient fluid and time, metasomatism is a viable mechanism to reset thermochronometers (Hay and Dempster 2009). Such petrologic considerations may help to explain the poor correlations between thermochronologic data and topography, and/or local faults, correlations that were hampered by imprecise data with poor reproducibility (e.g., Herman et al. 2009).

Surface uplift rates in the central Southern Alps have been estimated to range from 5 to 10 mm/yr (Wellman 1979; Bull and Cooper 1986; Norris and Cooper 2001). Early estimates of the amount of exhumation using FT data (Tippett and Kamp 1993; Kamp and Tippett 1993) were overestimated as compared to mass balance calculations based on plate convergence (Walcott 1998). It was subsequently realised that overestimates of the amount of exhumation had assumed that rock *P-T-t-D* paths during orogenesis were vertical, when in fact rock trajectories had significant horizontal components (Willett et al. 1993; Koons 1995; Walcott 1998). The style of orogenesis (see cross sections in Fig. 13.5) in the Southern Alps meant that rocks follow paths for long distances (and hence long durations) parallel or near-parallel to relevant isotherms, as compared to the distance and durations followed by rock paths perpendicular to relevant isotherms. In addition, isotherms are not everywhere parallel to the surface, and geothermal gradients evolve with time as heat is advected upwards towards the Alpine Fault. Rapid exhumation of hot, tectonically advected rocks along the Alpine Fault has resulted in transient, localised geothermal gradients of >125 °C/km in the upper 3–4 km of the crust (Sutherland et al. 2017).

Additional factors complicate determination of exhumation rates in the Southern Alps. Firstly, mineral equilibria modelling indicates that erosional exhumation of greywacke produces a continual supply of new fluid at temperatures as low as 400 °C and pressures <2 kbar, corresponding to <7 km depths (Vry et al. 2010). This means that there may be abundant fluids within the upper crust available to transport heat (e.g., Toy et al. 2010). Secondly, the presence of fluids may facilitate (re)crystallisation of micas at temperatures below their $T_c$ for argon. Micas may therefore recrystallise at much shallower depths than inferred "closure" depths calculated from assumed $T_c$ and assumed steady-state geothermal gradients. If crystallisation occurred at shallower depths than those assumed for $T_c$ and steady-state geothermal gradients, exhumation rates will be overestimated (Fig. 13.2c). Thirdly, microstructures and fluid inclusion data from the central Alpine fault zone indicate that quartz veins formed at relatively shallow crustal depths, with little variation in depths to relevant isotherms inferred for both hanging wall and fault rocks (Toy et al. 2010). In zones where thermochronologic data yield Alpine-related exhumation ages ($\leq$6 Ma in the Southern Alps), geobarometry is required to constrain the depth of crystallisation before exhumation rates can be calculated (Fig. 13.2).

Regional thermochronologic studies may mask effects due to localised recrystallisation, for example, due to late-stage hydrothermal alteration. What is generally lacking in studies on the Southern Alps is an understanding of rock particle paths obtained from *P-T-t-D* analyses on key samples. It is clear, however, that FT data are crucial to determine the timing of exhumation and brittle deformation as the Alpine fault zone evolved within the AUS-PAC plate boundary zone. To summarise, in the active AUS-PAC plate boundary in the South Island of New Zealand, partitioning of strain, erosion, mass wasting as well as the orographic effect of the Southern Alps continues to impact the landscape evolution of the range. Exhumation-related fluid flow may enhance syn-kinematic recrystallisation of minerals. Independent geobarometric data, to constrain the depth of mineral crystallisation, may be required before mineral ages can be interpreted with respect to the geodynamic evolution. While a wealth of thermochronologic data exists in the literature, sample sites are often scattered, and simple interpretations based on assumed $T_c$ may not be valid, especially given abundant evidence for fluid flow, and documented high geothermal gradients within the active plate-bounding fault zone.

## 13.7 Conclusions

Thermochronologic studies of plutonic and metamorphic rocks contribute quantitative data that provide insight into deep Earth processes. Successful application of thermochronologic methods to tectonics and geodynamics has been demonstrated through use of geologically and petrologically well-constrained sampling strategies, multiple methods applied to cogenetic minerals, and modelling using kinetic parameters to obtain continuous temperature–time histories. Case studies highlight the importance of FT thermochronology to determine the final exhumation of plutonic and metamorphic rocks within different tectonic and geodynamic settings:

- In (U)HP metamorphic terranes, the integration of petrologic data and multiple thermochronologic methods document prograde, peak, and retrograde *P-T-t-D* rock paths. FT thermochronology constrains the timing of final exhumation, thereby allowing assessment of whether (U)HP rocks were exhumed to the surface within the same subduction cycle that produced eclogite-facies rocks, and the mechanism(s) by which rocks were exhumed to near-surface P-T conditions.
- In extensional orogens, such as the TAM, AFT thermochronologic studies of samples collected in vertical profiles, across and along the range, offer the best approach to constrain the timing and rate of episodic cooling during rift flank development and landscape evolution.
- In intraplate collisional orogens, such as the Pyrenees mountains, best results are provided using a sampling strategy employing application of multiple low-temperature thermochronologic methods on cogenetic samples collected over a large range in elevation. This approach can constrain the timing of thrusting during orogenesis and the timing of subsequent exhumation. Data from age–elevation profiles, forward and inverse thermal modelling, and thermo-kinematic modelling are complementary, consistently revealing the sequence of orogenic events.
- In active transpressive plate boundary zones, such as the AUS-PAC plate boundary zone, FT thermochronology provides key constraints on timescales of orogenesis, geodynamic, and landscape evolution in the Southern Alps of New Zealand. However, the potential impact of hydrothermal fluid advection, on the (partial) resetting and annealing of fission tracks, may require re-evaluation of some geodynamic interpretations.

**Acknowledgements** SLB and PGF acknowledge support from the U. S. National Science Foundation. SLB and PGF thank J. Pettinga and the Erskine Program at the University of Canterbury. SLB thanks the Thonis family endowment. Thorough reviews by A. Blythe, M. Danišík, J. Gonzalez, T. Warfel, M. Jimenez, J.M. Brigham, N. Perez Consuegra, and R. Glas are greatly appreciated.

## References

Abers GA, Eilon Z, Gaherty JB, Jin G, Kim YH, Obrebski M, Dieck C (2016) Southeast Papuan crustal tectonics: imaging extension and buoyancy of an active rift. J Geophys Res Solid Earth 121:951–971

Adams CJ (1980) Uplift rates and thermal structure in the Alpine fault zone and Alpine schists, Southern Alps, New Zealand. Geol Soc London Spec Publ 9:211–222

Adams CJ, Gabites JE (1985) Age of metamorphism and uplift in the Haast schist group at Haast pass, Lake Wanaka and Lake Hawea, South Island, New Zealand. New Z J Geol Geophys 28:85–96

Ague JJ, Baxter EF (2007) Brief thermal pulses during mountain building recorded by Sr dif-fusion in apatite and multicomponent diffusion in garnet. Earth Planet Sci Lett 261:500–516

Amato JM, Johnson CM, Baumgartner LP, Beard BL (1999) Rapid exhumation of the Zermatt-Saas ophiolite deduced from high-precision Sm, Nd and Rb–Sr geochronology. Earth Planet Sci Lett 171:425–438

Baldwin SL (1996) Contrasting P-T-t histories for blueschists from the western Baja terrane and the Aegean: effects of synsubduction exhumation and backarc extension. In: Bebout GE, Scholl DW, Kirby SH, Platt JP (eds) Subduction top to bottom, American Geophysical Union, Washington, DC. https://doi.org/10.1029/GM096p0135

Baldwin SL, Das JP (2015) Atmospheric Ar and Ne returned from mantle depths to the Earth's surface by forearc recycling. Proc Nat Acad Sci 112:14174–14179

Baldwin SL, Harrison TM (1992) The P-T-t history of serpentinite matrix mélange from west-central Baja California. Geol Soc Am Bull 104:18–31

Baldwin SL, Lister GS, Hill EJ, Foster DA, McDougall I (1993) Thermochronologic con-straints on the tectonic evolution of active metamorphic core complexes, D'Entrecasteaux Islands, Papua New Guinea. Tectonics 12:611–628

Baldwin SL, Monteleone BD, Webb LE, Fitzgerald PG, Grove M, Hill EJ (2004) Pliocene eclogite exhumation at plate tectonic rates in eastern Papua New Guinea. Nature 431:263–267

Baldwin SL, Webb LE, Monteleone BD (2008) Late Miocene coesite-eclogite exhumed in the Woodlark Rift. Geology 36:735–738

Baldwin SL, Fitzgerald PG, Webb LE (2012) Tectonics of the New Guinea region. Annu Rev Earth Planet Sci 40:495–520

Balestrieri ML, Bigazzi G, Ghezzo C, Lombardo B (1994) Fission track dating of apatites from the Granite Harbour Instrusive suite and uplift-denduation history of the Transantarctic Mountains in the area between the Mariner and David Glaciers (Northern Victoria Land, Antarctica). Terra Antartica 1:82–87

Balestrieri ML, Bigazzi G, Ghezzo C (1997) Uplift—denudation of the Transantarctic Mountains between the david and the mariner glaciers, Northern Victoria Land (Antarctica): Constraints by apatite fission-track analysis. In: Ricci CA (ed) The Antarctic region: geological evolution and processes. Terra Antarctica Publication, Siena, pp 547–554

Barrett PJ (1965) Geology of the area between the Axel Heiberg and Shackleton Glaciers, Queen Maud Mountains, Antarctica. New Z J Geol Geophys 8:344–370

Barrett PJ (1979) Proposed drilling in McMurdo Sound—1979 Memoir of the National Institute of Polar Research. Special Issue 13:231–239

Barrett PJ (1991) The Devonian to Triassic Beacon Supergroup of the Transantarctic Mountains and correlatives in other parts of Antarctica. In: Tingey RJ (ed) The geology of Antarctica, vol 17. Oxford Monographs on Geology and Geophysics. Clarendon Press, Oxford, pp 120–152

Barrett PJ (1996) Antarctic paleoenvironment through Cenozoic times—a review. Terra Antarct 3:103–119

Barrett PJ, Elliot DH (1973) Reconnaissance geologic map of the Buckley Island Quadrangle, Transantarctic Mountains. Antarctica, United States Geological Survey, Reston, Va

Batt GE, Kohn BP, Braun J, McDougall I, Ireland TR (1999) New insight into the dynamic development of the Southern Alps, New Zealand, from detailed thermochronological investigation of the Mataketake Range pegmatites. Geol Soc London Spec Publ 154:261–282

Batt GE, Braun J, Kohn BP, McDougall I (2000) Thermochronological analysis of the dynamics of the Southern Alps, New Zealand. Geol Soc Am Bull 112:250–266

Batt GE, Baldwin SL, Cottam M, Fitzgerald PG, Brandon M (2004) Cenozoic plate boundary evolution in the South Island of New Zealand: New thermochronological constraints. Tectonics 23: TC4001

Beavan J, Tregoning P, Bevis M, Kato T, Meertens C (2002) Motion and rigidity of the Pacific Plate and implications for plate boundary deformation. J Geophys Res Solid Earth 107

Beavan J, Ellis S, Wallace LM, Denys P (2007) Kinematic constraints from GPS on oblique convergence of the Pacific and Australian plates, central South Island, New Zealand. In: Okaya D, Stern TA, Davey FJ (eds) A Continental Plate Boundary: Tectonics at South Island, New Zealand, vol 175. American Geophysical Union. Washington, DC, pp 75–94

Beavan J, Denys P, Denham M, Hager B, Herring T, Molnar P (2010) Distribution of present-day vertical deformation across the Southern Alps, New Zealand, from 10 years of GPS data. Geophys Res Lett 37

Becker H (1993) Garnet peridotite and eclogite Sm–Nd mineral ages from the Lepontine dome (Swiss Alps): New evidence for Eocene high-pressure metamorphism in the central Alps. Geology 21:599–602

Berástegui X, García JM, Losantos M (1990) Structure and sedimentary evolution of the Organyà basin (Central South Pyrenean Unit, Spain) during the Lower Cretaceous. Bull Soc Géol Fr 8:251–264

Beucher R, Beek P, Braun J, Batt GE (2012) Exhumation and relief development in the Pelvoux and Dora-Maira massifs (western Alps) assessed by spectral analysis and inversion of thermochronological age transects J Geophys Res Earth Surface 117

Bialas RW, Buck WR, Studinger M, Fitzgerald PG (2007) Plateau collapse model for the Transantarctic Mountains-West Antarctic Rift system: insights from numerical experiments. Geology 35:687

Blythe AE (1998) Active tectonics and ultrahigh-pressure rocks. In Hacker BR, Liou JG (eds) When continents collide: geodynamics and geochemistry of ultrahigh-pressure rocks. Springer Netherlands, pp 141–160

Blythe AE, Huerta AD, Utevsky E (2011) Evaluating the Mesozoic West Antarctic Plateau col-lapse hypothesis: results from apatite fission-track and (U–Th)/He analyses from Byrd Glacier Outlet. In: AGU Fall Meeting Abstracts, 2011

Bohlen SR, Valley JW, Essene EJ (1985) Metamorphism in the Adirondacks. I. petrology, pressure and temperature. J Petrol 26:971–992

Braun J (2002) Quantifying the effect of recent relief changes on age-elevation relationships. Earth Planet Sci Lett 200:331–343

Brouwer FM, Van De Zedde DMA, Wortel MJR, Vissers RLM (2004) Late-orogenic heating during exhumation: Alpine PTt trajectories and thermomechanical models. Earth Planet Sci Lett 220:185–199

Brown RW, Summerfield MA (1997) Some uncertainties in the derivation of rates of denudation from thermochronologic data. Earth Surf Proc Land 22:239–248

Bull WB, Cooper AF (1986) Uplifted marine terraces along the Alpine fault, New Zealand. Sci-ence 234:1225–1228

Camacho A, Lee JKW, Hensen BJ, Braun J (2005) Short-lived orogenic cycles and the eclogitization of cold crust by spasmodic hot fluids. Nature 435:1191

Cape Roberts Science Team (2000) Studies from the Cape Roberts Project, Ross Sea Antarctica. Initial report on CRP-3 vol 7. Terra Antartica, vol 1/2. Terra Antartica Publication, Siena, Italy

Capponi G, Messiga B, Piccardo GB, Scambelluri M, Traverso G, Vannucci R (1990) Meta-morphic assemblages in layered amphibolites and micaschists from the Dessent Formation (Mountaineer Range, Antarctica). Mem Soc Geol Ital 43:87–95

Carswell DA, Brueckner HK, Cuthbert SJ, Mehta K, O'Brien PJ (2003) The timing of stabilisa-tion and the exhumation rate for ultra-high pressure rocks in the Western Gneiss Region of Norway. J Metam Geol 21:601–612

Chamberlain CP, Zeitler PK, Cooper AF (1995) Geochronologic constraints of the uplift and metamorphism along the Alpine Fault, South Island, New Zealand. New Z J Geol Geophys 38:515–523

Chamberlain CP, Shelly DR, Townend J, Stern TA (2014) Low-frequency earthquakes reveal punctuated slow slip on the deep extent of the Alpine fault, New Zealand. Geochem Ge-ophys Geosyst 15:2984–2999

Chopin C (1984) Coesite and pure pyrope in high-grade blueschists of the Western Alps: a first record and some consequences. Contrib Mineral Petr 86:107–118. https://doi.org/10.1007/BF00381838

Chopin C, Henry C, Michard A (1991) Geology and petrology of the coesite-bearing terrain, Dora Maira massif, Western Alps. Eu J Miner 3:263–291
Coleman RG, Wang X (1995) Overview of the geology and tectonics of UHPM. Ultrahigh pressure metamorphism, pp 1–32
Compagnoni R, Hirajima T, Chopin C (1995) Ultra-high-pressure metamorphic rocks in the Western Alps. Ultrahigh pressure metamorphism, pp 206–243
Coney PJ, Muñoz JA, McClay K, Evenchick CA (1996) Syn-tectonic burial and post-tectonic exhumation of an active foreland thrust belt, southern Pyrenees, Spain. J Geol Soc 153:9–16
Cooper AF (1972) Progressive metamorphism of metabasic rocks from the Haast Schist Group of southern New Zealand. J Petrol 13:457–492
Cooper AF (1974) Multiphase deformation and its relationship to metamorphic crystallisation at Haast River, South Westland, New Zealand. New Z J Geol Geophys 17:855–880
Cox SC, Sutherland R (2007) Regional geological framework of South Island, New Zealand, and is significance for understanding the active plate boundary. In: Okaya D, Stern TA, Davey FJ (eds) A Continental Plate Boundary: Tectonics at South Island, New Zealand, vol 175. American Geophysical Union, Washington, DC, pp 19–46. https://doi.org/10.1029/175gm03
Dachs E, Proyer A (2002) Constraints on the duration of high-pressure metamorphism in the Tauern Window from diffusion modelling of discontinuous growth zones in eclogite garnet. J Metam Geol 20:769–780
Dalziel IWD (1992) Antarctica: a tale of two supercontinents. Annu Rev Earth Planet Sci 20:501–526
Davies HL, Warren RG (1988) Origin of eclogite-bearing, domed, layered metamorphic com-plexes ("core complexes") in the D'Entrecasteaux Islands, Papua New Guinea. Tectonics 7:1–21
de Sigoyer J, Chavagnac V, Blichert-Toft J, Villa IM, Luais B, Guillot S, Cosca M, Mascle G (2000) Dating the Indian continental subduction and collisional thickening in the northwest Himalaya: Multichronology of the Tso Morari eclogites. Geology 28:487–490
DesOrmeau JW, Gordon SM, Kylander-Clark ARC, Hacker BR, Bowring SA, Schoene B, Sam-perton KM (2015) Insights into (U) HP metamorphism of the Western Gneiss Region, Norway: a high-spatial resolution and high-precision zircon study. Chem Geol 414:138–155
Dewey JF (2005) Orogeny can be very short. Proc Nat Acad Sci 102:15286–15293
Dodson MH (1973) Closure temperatures in cooling geochronological and petrological systems. Contrib Mineral Petr 40:259–274
Ducea MN (2016) RESEARCH FOCUS: understanding continental subduction: a work in progress. Geology 44:239–240
Duchene S, Lardeaux J-M, Albarède F (1997) Exhumation of eclogites: insights from depth-time path analysis. Tectonophysics 280:125–140
Dunlap WJ, Teyssier C, McDougall I, Baldwin S (1995) Thermal and structural evolution of the intracratonic Arltunga Nappe Complex, central Australia. Tectonics 14:1182–1204
Elliot DH (1975) Tectonics of Antarctica: a review. Am J Sci 275:45–106
Elliot DH (1992) Jurassic magmatism and tectonism associated with Gondwanaland break-up; an Antarctic perspective. Geol Soc London Spec Publ 68:165–184
Elliot DH, Fleming TH (2004) Occurrence and dispersal of magmas in the Jurassic Ferrar large igneous province, Antarctica. Gondwana Res 7:223–237
Ellis SM, Little TA, Wallace LM, Hacker BR, Buiter SJH (2011) Feedback between rifting and diapirism can exhume ultrahigh-pressure rocks. Earth Planet Sci Lett 311:427–438
England PC, Thompson AB (1984) Pressure-temperature-time paths of regional metamor-phism I. Heat transfer during the evolution of regions of thickened continental crust. J Petrol 25:894–928
Ernst WG (1988) Tectonic history of subduction zones inferred from retrograde blueschist PT paths. Geology 16:1081–1084
Fillon C, van der Beek P (2012) Post-orogenic evolution of the southern Pyrenees: constraints from inverse thermo-kinematic modelling of low-temperature thermochronology data. Basin Res 24:418–436
Fitzgerald PG (1992) The Transantarctic Mountains of southern Victoria Land: the application of apatite fission track analysis to a rift shoulder uplift. Tectonics 11:634–662
Fitzgerald PG (1994) Thermochronologic constraints on post-Paleozoic tectonic evolution of the central Transantarctic Mountains, Antarctica. Tectonics 13:818–836
Fitzgerald PG (2002) Tectonics and landscape evolution of the Antarctic plate since Gondwana breakup, with an emphasis on the West Antarctic rift system and the Transantarctic Mountains. In: Gamble JA, Skinner DNB, Henrys S (eds) Antarctica at the close of a Millennium. In: Proceedings of the 8th international symposium on Antarctic earth science. The Royal Society of New Zealand Bulletin, 35 edn. Royal Society of New Zealand, pp 453–469
Fitzgerald PG, Baldwin SL (2007) Thermochronologic constraints on Jurassic rift flank denudation in the Thiel Mountains, Antarctica. In: Cooper AK, Raymond CR et al. (eds) Antarctica: a keystone in a changing world. USGS open-file report 2007
Fitzgerald PG, Baldwin SL (1997) Detachment fault model for the evolution of the Ross Embayment: geologic and fission track constraints from DSDP site 270. In: Ricci CA (ed) The Antarctic region: geological evolution and processes. Terra Antarctica Publication, Siena, pp. 555–564
Fitzgerald PG, Gleadow AJW (1988) Fission-track geochronology, tectonics and structure of the Transantarctic Mountains in northern Victoria Land, Antarctica. Chem Geol Isotope Geosci Sect 73:169–198
Fitzgerald PG, Gleadow AJW (1990) New approaches in fission track geochronology as a tectonic tool: examples from the Transantarctic Mountains. Nucl Tracks 17:351–357
Fitzgerald PG, Malusà MG (2018) Chapter 9: concept of the exhumed partial annealing (retention) zone and age-elevation profiles in thermochronology. In: Malusà MG, Fitzgerald PG (eds) Fission-track thermochronology and its application to geology. Springer
Fitzgerald PG, Stump E (1997) Cretaceous and Cenozoic episodic denudation of the Transantarctic Mountains, Antarctica: new constraints from apatite fission track thermochronology in the Scott Glacier region. J Geophys Res 102:7747–7765
Fitzgerald PG, Muñoz JA, Coney PJ, Baldwin SL (1999) Asymmetric exhumation across the Pyrenean orogen: implications for the tectonic evolution of collisional orogens. Earth Planet Sci Lett 173:157–170
Fitzgerald PG, Baldwin SL, O'Sullivan PB, Webb LE (2006) Interpretation of (U–Th)/He single grain ages from slowly cooled crustal terranes: a case study from the Transantarctic Mountains of southern Victoria Land. Chem Geol 225:91–120
Fitzgerald PG, Baldwin SL, Bermúdez MB, Webb LE, Little TA, Miller SR, Malusa MG, Seward D (2015) Exhumation of the Papuan New Guinea (U)HP terrane: constraints from low temperature thermochronology. XI International Eclogite Conference, Dominican Republic. http://www.ruhr-uni-bochum.de/eclogite/iec11/IEC-2015-abstract-volume.pdf
Frezzotti ML, Selverstone J, Sharp ZD, Compagnoni R (2011) Carbonate dissolution during subduction revealed by diamond-bearing rocks from the Alps. Nature Geosci 4:703

Gebauer D (1996) A P-T-t Path for an (ultra?) High-Pressure ultramafic/mafic rock association and its felsic country-rocks based on SHRIMP dating of magmatic and metamorphic zircon domains. example: Alpe Arami (Central Swiss Alps). Earth Proc: Read Isotopic Code 307–329

Gebauer D, Schertl HP, Brix M, Schreyer W (1997) 35 Ma old ultrahigh-pressure metamorphism and evidence for very rapid exhumation in the Dora Maira Massif, Western Alps. Lithos 41:5–24

Gibson M, Sinclair HD, Lynn GJ, Stuart FM (2007) Late- to post-orogenic exhumation of the central Pyrenees revealed through combined thermochronological data and thermal modeling. Basin Res 19:323–334

Gilotti JA (2013) The realm of ultrahigh-pressure metamorphism. Elements 9:255–260

Gleadow AJW, Brown RW (2000) Fission track thermochronology and the long term denuda-tional response to tectonics. In: Summerfield MA (ed) Geomorphology and global tectonics. John Willey and Sons, New York, pp 57–75

Gleadow AJW, Fitzgerald PG (1987) Uplift history and structure of the Transantarctic Mountains: new evidence from fission track dating of basement apatites in the Dry Valleys area, southern Victoria Land. Earth Planet Sci Lett 82:1–14

Gleadow AJW, McKelvey BC, Ferguson KU (1984) Uplift history of the Transantarctic Mountains in the Dry Valleys area, southern Victoria Land, Antarctica, from apatite fission track ages. New Z J Geol Geophys 27:457–464

Goldstein RH, Reynolds TJ (1994) Systematics of fluid inclusions in diagenetic minerals. SEPM Short Course 31, Tulsa, 199 pp

Goodge JW (2007) Metamorphism in the Ross orogen and its bearing on Gondwana margin tectonics. Geol S Am S 419:185–203

Gordon SM, Little TA, Hacker BR, Bowring SA, Korchinski M, Baldwin SL, Kylander-Clark ARC (2012) Multi-stage exhumation of young UHP–HP rocks: timescales of melt crystallization in the D'Entrecasteaux Islands, southeastern Papua New Guinea. Earth Planet Sci Lett 351–352:237–246

Grapes R, Watanabe T (1992) Metamorphism and uplift of Alpine schist in the Franz Josef-Fox Glacier area of the Southern Alps, New Zealand. J Metam Geol 10:171–180

Guillot S, Hattori K, Agard P, Schwartz S, Vidal O (2009) Exhumation processes in oceanic and continental subduction contexts: a review. In: Subduction Zone Geodynamics. Springer, pp 175–205

Gunn BM, Warren G (1962) Geology of Victoria Land between the Mawson and Mulock Glaciers, Antarctica vol 70–71. New Z Geol Survey Bull, Lower Hutt

Hacker BR (2006) Pressures and temperatures of ultrahigh-pressure metamorphism: implications for UHP tectonics and $H_2O$ in subducting slabs. Int Geol Rev 48:1053–1066

Hacker BR, Ratschbacher L, Webb LE, Ireland T, Walker D, Shuwen D (1998) U/Pb zircon ages constrain the architecture of the ultrahigh-pressure Qinling-Dabie Orogen, China. Earth Planet Sci Lett 161:215–230

Hacker BR, Ratschbacher L, Webb LE, McWilliams MO, Ireland T, Calvert A, Dong S, Wenk HR, Chateigner D (2000) Exhumation of ultrahigh-pressure continental crust in east central China: late Triassic-Early Jurassic tectonic unroofing. J Geophys Res Solid Earth 105:13339–13364

Harlov DE (2015) Apatite: a fingerprint for metasomatic processes. Elements 11:171–176

Harlov DE, Wirth R, Förster H-J (2005) An experimental study of dissolution–reprecipitation in fluorapatite: fluid infiltration and the formation of monazite. Contrib Mineral Petr 150:268–286

Harrison TM, Zeitler PK (2005) Fundamentals of noble gas thermochronometry. Rev Mineral Geochem 58:123–149

Hay D, Dempster T (2009) Zircon behaviour during low-temperature metamorphism. J Petrol 50:571–589

Heimann A, Fleming TH, Elliot DH, Foland KA (1994) A short interval of Jurassic continental flood basalt volcanism in Antarctica as demonstrated by $^{40}Ar/^{39}Ar$ geochronology. Earth Planet Sci Lett 121:19–41

Herman F, Cox S, Kamp P (2009) Low-temperature thermochronology and thermokinematic modeling of deformation. Tectonics

Hill EJ, Baldwin SL (1993) Exhumation of high-pressure metamorphic rocks during crustal extension in the D'Entrecasteaux region, Papua New Guinea. J Metam Geol 11:261–277

Hill EJ, Baldwin SL, Lister GS (1992) Unroofing of active metamorphic core complexes in the D'Entrecasteaux Islands, Papua New Guinea. Geology 20:907–910

Hodges KV (1991) Pressure-temperature-time paths. Annu Rev Earth Planet Sci 19:207–236

Houlié N, Stern TA (2012) A comparison of GPS solutions for strain and SKS fast directions: Implications for modes of shear in the mantle of a plate boundary zone. Earth Planet Sci Lett 345:117–125

Hu S, Kohn BP, Raza A, Wang J, Gleadow AJW (2006) Cretaceous and Cenozoic cooling history across the ultrahigh pressure Tongbai-Dabie belt, central China, from apatite fission-track thermochronology. Tectonophysics 420:409–429

Huntington KW, Ehlers TA, Hodges KV, Whipp DM (2007) Topography, exhumation pathway, age uncertainties, and the interpretation of thermochronometer data. Tectonics 26

Husson L, Moretti I (2002) Thermal regime of fold and thrust belts—an application to the Bolivian subAndean zone. Tectonophysics 345:253–280

Jamieson RA, Beaumont C (2013) On the origin of orogens. Geol Soc Am Bull 125:1671–1702

Jiracek GR, Gonzalez VM, Grant Caldwell T, Wannamaker PE, Kilb D (2007) Seismogenic, electrically conductive, and fluid zones at continental plate boundaries in New Zealand, Himalaya, and California, USA. In: O'kaya D, Stern TA, Davey F (eds) A Continental Plate Boundary: Tectonics at South Island, New Zealand, vol 175. American Geophysical Union, Washington DC, pp 347–369

Jolivet M, Labaume P, Brunel M, Arnaud N, Campani M (2007) Thermochronology constraints for the propagation sequence of the south Pyrenean basement thrust system (France-Spain). Tectonics 26: TC5007

Kamp PJJ, Tippett JM (1993) Dynamics of Pacific plate crust in the South Island (New Zealand) zone of oblique continent-continent convergence. J Geophys Res Solid Earth 98:16105–16118

Kamp PJJ, Green PF, White SH (1989) Fission track analysis reveals character of collisional tectonics in New Zealand. Tectonics 8:169–195

Ketcham R (2018) Chapter 3. Fission track annealing: from geologic observations to thermal history modeling. In: Malusà MG, Fitzgerald PG (eds) Fission-track thermochronology and its application to geology. Springer

Kohn B, Chung L, Gleadow A (2018) Chapter 2. Fission-track analysis: field collection, sample preparation and data acquisition. In: Malusà MG, Fitzgerald PG (eds) Fission-track thermochronology and its application to geology. Springer

Kohn MJ (2016) Metamorphic chronology-a tool for all ages. Am Mineral 101:25–42

Kohn MJ, Corrie SL, Markley C (2015) The fall and rise of metamorphic zircon. Am Mineral 100:897–908

Koons PO (1995) Modeling the topographic evolution of collisional belts. Annu Rev Earth Planet Sci 23:375–408

Ksienzyk AK, Dunkl I, Jacobs J, Fossen H, Kohlmann F (2014) From orogen to passive margin: constraints from fission track and (U–

Th)/He analyses on Mesozoic uplift and fault reactivation in SW Norway. Geol Soc London Spec Publ 390(SP390):327

Kufner S-K, Schurr B, Sippl C, Yuan X, Ratschbacher L, Ischuk A, Murodkulov S, Schneider F, Mechie J, Tilmann F (2016) Deep India meets deep Asia: Lithospheric indentation, delamination and break-off under Pamir and Hindu Kush (Central Asia). Earth Planet Sci Lett 435:171–184

Lardeaux J-M, Schwartz S, Tricart P, Paul A, Guillot S, Béthoux N, Masson F (2006) A crustal-scale cross-section of the south-western Alps combining geophysical and geological imagery. Terra Nova 18:412–422

Leech ML, Stockli DF (2000) The late exhumation history of the ultrahigh-pressure Maksyutov Complex, south Ural Mountains, from new apatite fission track data. Tectonics 19:153–167

LeMasurier WE, Thomson JW (eds) (1990) Volcanoes of the Antarctic Plate and Southern Oceans. Antarctic research series, vol 48. American Geophysical Union, Washington, DC

Lennykh VI, Valizer PM, Beane R, Leech M, Ernst WG (1995) Petrotectonic evolution of the Maksyutov Complex, Southern Urals, Russia: implications for ultrahigh-pressure meta-morphism. Int Geol Rev 37:584–600

Liao J, Malusà MG, Liang Z, Baldwin SL, Fitzgerald PG, Gerya T (2018) Divergent plate motion drives rapid exhumation of (ultra) high pressure rocks. Earth Planet Sci Lett 491:67–80. https://doi.org/10.1016/j.epsl.2018.03.024

Lindsay JF, Gunner J, Barrett PJ (1973) Reconnaissance geologic map of the Mount Elizabeth and Mount Kathleen quadrangles, Transantarctic Mountains, Antarctica. US Geological Survey Washington, DC, 1:250,000

Liou JG, Ernst WG, Zhang RY, Tsujimori T, Jahn BM (2009) Ultrahigh-pressure minerals and metamorphic terranes—the view from China. J Asian Earth Sci 35:199–231

Lisker F (2002) Review of fission track studies in northern Victoria Land, Antarctica; passive margin evolution versus uplift of the Transantarctic Mountains. Tectonophysics 349:57–73

Little TA, Cox SE, Vry JK, Batt G (2005) Variations in exhumation level and uplift rate along the obliqu-slip Alpine fault, central Southern Alps. New Zealand. Geol Soc Am Bull 117:707

Little TA, Baldwin SL, Fitzgerald PG, Monteleone BM (2007) Continental rifting and meta-morphic core complex formation ahead of the Woodlark Spreading Ridge, D'Entrecasteaux Islands, Papua New Guinea. Tectonics 26: TC1002. doi:1010.1029/2005TC001911

Liu LP, Li Z-X, Danišík M, Li S, Evans N, Jourdan F, Tao N (2017) Thermochronology of the Sulu ultrahigh-pressure metamorphic terrane: implications for continental collision and lithospheric thinning. Tectonophysics 712:10–29

Lock J, Willett S (2008) Low-temperature thermochronometric ages in fold-and-thrust belts. Tectonophysics 456:147–162

Lovera OM, Richter FM, Harrison TM (1989) The 40Ar/39Ar thermochrometry for slowly cooled samples having a distribution of diffusion domain sizes. J Geophys Res 94:17917–17935

Lovera OM, Grove M, Harrison TM, Mahon KI (1997) Systematic analysis of K-feldspar 40Ar 39Ar step heating results: I. Significance of activation energy determinations. Geochim Cosmochim Ac 61:3171–3192

Lovera OM, Grove M, Harrison TM (2002) Systematic analysis of K-feldspar $^{40}Ar/^{39}Ar$ step heating results II: Relevance of laboratory argon diffusion properties to nature. Geochim Cosmochim Ac 66:1237–1255

Malusà MG, Fitzgerald PG (2018a) Chapter 8. From cooling to exhumation: setting the reference frame for the interpretation of thermochronologic data. In: Malusà MG, Fitzgerald PG (eds) Fission-track thermochronology and its application to geology. Springer

Malusà MG, Fitzgerald PG (2018b) Chapter 10. Application of thermochronology to geologic problems: bedrock and detrital approaches. In: Malusà MG, Fitzgerald PG (eds) Fission-track thermochronology and its application to geology. Springer

Malusà MG, Polino R, Zattin M, Bigazzi G, Martin S, Piana F (2005) Miocene to present differential exhumation in the Western Alps: insights from fission track thermochronology. Tectonics 24:1–23 TC3004

Malusà MG, Philippot P, Zattin M, Martin S (2006) Late stages of exhumation constrained by structural, fluid inclusion and fission track analyses (Sesia–Lanzo unit, Western European Alps). Earth Planet Sci Lett 243:565–580

Malusà MG, Faccenna C, Garzanti E, Polino R (2011) Divergence in subduction zones and exhumation of high pressure rocks (Eocene Western Alps). Earth Planet Sci Lett 310:21–32

Malusà MG, Faccenna C, Baldwin SL, Fitzgerald PG, Rossetti F, Balestrieri ML, Danišík M, El-lero A, Ottria G, Piromallo C (2015) Contrasting styles of (U) HP rock exhumation along the Cenozoic Adria-Europe plate boundary (Western Alps, Calabria, Corsica). Geochem Geophys Geosyst 16:1786–1824

McClay K, Muñoz J-A, García-Senz J (2004) Extensional salt tectonics in a contractional orogen: a newly identified tectonic event in the Spanish Pyrenees. Geology 32:737–740

McDougall I, Harrison TM (1999) Geochronology and thermochronology by the $^{40}Ar/^{39}Ar$ method vol 9. Oxford Monographs on Geology and Geophysics, 2nd edn. Oxford University Press, New York

Metcalf JR, Fitzgerald PG, Baldwin SL, Muñoz JA (2009) Thermochronology in a convergent orogen: constraints on thrust faulting and exhumation from the Maladeta Pluton in the Axial Zone of the Central Pyrenees. Earth Planet Sci Lett 287:488–503

Miller SR, Fitzgerald PG, Baldwin SL (2010) Cenozoic range-front faulting and development of the Transantarctic Mountains near Cape Surprise, Antarctica: Thermochronologic and geo-morphologic constraints. Tectonics 29. https://doi.org/10.1029/2009tc002457

Monteleone BD, Baldwin SL, Webb LE, Fitzgerald PG, Grove M, Schmitt A (2007) Late Miocene-Pliocene eclogite-facies metamorphism, D'Entrecastreaux Islands, SE Papua New Guinea. J Metam Geol 25:245–265

Morris RG, Sinclair HD, Yelland AJ (1998) Exhumation of the Pyrenean orogen: implications for sediment discharge. Basin Res 10:69–85

Muñoz JA (1992) Evolution of a continental collision belt: ECORS Pyrenees crustal balanced cross-section. In: McClay K (ed) Thrust Tectonics. Chapman and Hall, London, pp 235–246

Muñoz JA (2002) The Pyrenees Alpine tectonics; I, The Alpine system north of the Betic Cor-dillera. In: Gibbons W, Moreno T (eds) The geology of Spain. The Geological Society, London, p 649

Nagel TJ (2008) Tertiary subduction, collision and exhumation recorded in the Adula nappe, central Alps. Geol Soc London Spec Publ 298:365–392

Norris RJ, Cooper AF (2001) Late Quaternary slip rates and slip partitioning on the Alpine Fault, New Zealand. J Struct Geol 23:507–520

Olivetti V, Balestrieri ML, Rossetti F, Talarico FM (2013) Tectonic and climatic signals from apatite detrital fission track analysis of the Cape Roberts Project core records, South Victoria Land, Antarctica. Tectonophysics 594:80–90

Pedersen VK, Huismans RS, Moucha R (2016) Isostatic and dynamic support of high topography on a North Atlantic passive margin. Earth Planet Sci Lett 446:1–9

Petersen KD, Buck WR (2015) Eduction, extension, and exhumation of ultrahigh-pressure rocks in metamorphic core complexes due to subduction initiation. Geochem Geophys Geosyst 16:2564–2581

Petford N, Cruden AR, McCaffrey KJW, Vigneresse JL (2000) Granite magma formation, transport and emplacement in the Earth's crust. Nature 408:669

Philpotts A, Ague J (2009) Principles of igneous and metamorphic petrology. Cambridge University Press

Powell R, Holland T (2010) Using equilibrium thermodynamics to understand metamorphism and metamorphic rocks. Elements 6:309–314

Puigdefàbregas C, Souquet P (1986) Tectonostratigraphic cycles and depositional sequences of the Mesozoic and Tertiary from the Pyrenees. Tectonophysics 129:173–203

Purdy JW, Jager E (1976) K–Ar ages on rock forming minerals from Central Alps. Mem Univ Padova 30

Rasmussen B (2005) Zircon growth in very low grade metasedimentary rocks: evidence for zirconium mobility at ~250 °C. Contrib Mineral Petr 150:146–155

Ratschbacher L, Hacker BR, Webb LE, McWilliams M, Ireland T, Dong S, Calvert A, Chateigner D, Wenk HR (2000) Exhumation of the ultrahigh-pressure continental crust in east central China: Cretaceous and Cenozoic unroofing and the Tan-Lu fault. J Geophys Res Solid Earth 105:13303–13338

Reiners PW, Zhou Z, Ehlers TA, Changhai X, Brandon MT, Donelick RA, Nicolescu S (2003) Post-orogenic evolution of the Dabie Shan, eastern China, from (U–Th)/He and fission track thermochronology. Am J Sci 303:489–518

Ring U, Uysal IT, Glodny J, Cox SC, Little T, Thomson SN, Stubner K, Bozkaya O (2017) Faultgouge dating in the Southern Alps, New Zealand. Tectonophysics 717:321–338

Rohrman M, Beek P, Andriessen P, Cloetingh S (1995) Meso-Cenozoic morphotectonic evolution of southern Norway: Neogene domal uplift inferred from apatite fission track thermo-chronology. Tectonics 14:704–718

Rubatto D (2017) Zircon: the metamorphic mineral. Rev Min Geochem 83:261–295

Rubatto D, Hermann J (2001) Exhumation as fast as subduction? Geology 29:3–6

Rubatto D, Gebauer D, Fanning M (1998) Jurassic formation and Eocene subduction of the Zermatt-Saas-Fee ophiolites: implications for the geodynamic evolution of the Central and Western Alps. Contrib Mineral Petr 132:269–287

Ryan WBF, Carbotte SM, Coplan JO, O'Hara S, Melkonian A, Arko R, Weissel RA, Ferrini V, Goodwillie A, Nitsche F, Bonczkowski J, Zemsky R (2009) Global multi-resolution topography synthesis. Geochem Geophys Geosyst 10. https://doi.org/10.1029/2008gc002332

Sawyer EW, Cesare B, Brown M (2011) When the continental crust melts. Elements 7:229–234

Schertl H-P, Schreyer W, Chopin C (1991) The pyrope-coesite rocks and their country rocks at Parigi, Dora Maira Massif, Western Alps: detailed petrography, mineral chemistry and PT-path. Contrib Mineral Petr 108:1–21

Schlup M, Carter A, Cosca M, Steck A (2003) Exhumation history of eastern Ladakh revealed by 40Ar/39Ar and fission-track ages: the Indus River-Tso Morari transect. NW Himalaya J Geol Soc 160:385–399

Seguret M (1972) Etude tectonique des nappes et séries décollées de la partie centrale du ver-sant sud des Pyrénées Pub Ustela, Géol Struct, pp 155

Selverstone J, Sprear F (1985) Metamorphic P-T Paths from pelitic schists and greenstones from the south-west Tauern Window, Eastern Alps. J Metam Geol 3:439–465

Selverstone J, Spear FS, Franz G, Morteani G (1984) High-pressure metamorphism in the SW Tauern Window, Austria: PT paths from hornblende-kyanite-staurolite schists. J Petrol 25:501–531

Sheppard DS, Adams CJ, Bird GW (1975) Age of metamorphism and uplift in the Alpine Schist Belt, New Zealand. Geol Soc Am Bull 86:1147–1153

Smith DC (1984) Coesite in clinopyroxene in the Caledonides and its implications for geodynamics. Nature 310:641–644

Solarino S, Malusà MG, Eva E, Guillot S, Paul A, Schwartz S, Zhao L, Aubert C, Dumont T, Pondrelli S, Salimbeni S, Wang Q, Xu X, Zheng T, Zhu R (2018) Mantle wedge exhumation beneath the Dora-Maira (U)HP dome unravelled by local earthquake tomography (Western Alps). Lithos 296–299:623–636

Spear FS (1993) Metamorphic phase equilibria and pressure-temperature-time paths. Min Soc Am, Washington, DC

Spear FS (2014) The duration of near-peak metamorphism from diffusion modelling of garnet zoning. J Metam Geol 32:903–914

Stern T, ten Brink US (1989) Flexural uplift of the Transantarctic Mountains. J Geophys Res 94:10315–10330

Stern TA, Okaya D, Kleffmann S, Scherwath M, Henrys S, Davey FJ (2007) Geophysical exploration and dynamics of the Alpine Fault zone. In: Okaya D, Stern TA, Davey FJ (eds) A Continental Plate Boundary: Tectonics at South Island, New Zealand, vol 175. American Geophysical Union, Washington, DC, pp 207–233. https://doi.org/10.1029/175gm11

Stump E, Fitzgerald PG (1992) Episodic uplift of the Transantarctic Mountains. Geology 20:161

Sutherland R, Townend J, Toy V, Upton P, Coussens J, Allen M, Baratin L-M, Barth N, Becroft L, Boese C (2017) Extreme hydrothermal conditions at an active plate-bounding fault. Nature 546:137–140

ter Voorde M, de Bruijne CH, Cloetingh SAPL, Andriessen PAM (2004) Thermal consequences of thrust faulting: simultaneous versus successive fault activation and exhumation. Earth Planet Sci Lett 223:395–413

Tippett JM, Kamp PJJ (1993) Fission track analysis of the late Cenozoic vertical kinematics of continental Pacific crust, South Island, New Zealand. J Geophys Res Solid Earth 98:16119–16148

Toy VG, Prior DJ, Norris RJ (2008) Quartz fabrics in the Alpine Fault mylonites: Influence of pre-existing preferred orientations on fabric development during progressive uplift. J Struct Geol 30:602–621

Toy VG, Craw D, Cooper AF, Norris RJ (2010) Thermal regime in the central Alpine Fault zone, New Zealand: constraints from microstructures, biotite chemistry and fluid inclusion data. Tectonophysics 485:178–192

Tracy RJ, Robinson P (1980) Evolution of metamorphic belts: information from detailed petrologic studies. The Caledonides in the USA 2:189–196

Vannucci G, Piazza M, Pastorino P, Fravega P (1997) Le facies a coralli coloniali e rodoficee calcaree di alcune sezioni basali della Formazione di Molare (Oligocene del Bacino Terziario del Piemonte. Italia nord-occidentale Mem Atti Soc Toscana Sci Nat, Ser A 104:1–27

Vergés J, Fernàndez M, Martínez A (2002) The Pyrenean orogen: pre-, syn-, and post-collisional evolution. J Virtual Expl 8:55–84

Viete DR, Hermann J, Lister GS, Stenhouse IR (2011) The nature and origin of the Barrovian metamorphism, Scotland: diffusion length scales in garnet and inferred thermal time scales. J Geol Soc 168:115–132

Vry JK, Baker J, Maas R, Little T, Grapes R, Dixon M (2004) Zoned (Cretaceous and Cenozoic) garnet and the timing of high grade metamorphism, Southern Alps, New Zealand. J Metam Geol 22:137–157

Vry J, Powell R, Golden KM, Petersen K (2010) The role of exhumation in metamorphic dehydration and fluid production. Nature Geosci 3:31

Walcott RI (1998) Modes of oblique compression: late Cenozoic tectonics of the South Island of New Zealand. Rev Geophys 36:1–26

Wallace LM, Beavan J, McCaffrey R, Berryman K, Denys P (2006) Balancing the plate motion budget in the South Island, New Zealand using GPS, geological and seismological data. Geophys J Int. https://doi.org/10.1111/j.1365-246X.2006.03183.x

Walsh EO, Hacker BR (2004) The fate of subducted continental margins: two-stage exhumation of the high-pressure to ultrahigh-pressure Western Gneiss Region, Norway. J Metam Geol 22:671–687

Warren-Smith E, Lamb S, Seward D, Smith E, Herman F, Stern T (2016) Thermochronological evidence of a low-angle, mid-crustal detachment plane beneath the central South Island, New Zealand. Geochem Geophys Geosyst 17:4212–4235

Webb LE, Baldwin SL, Little TA, Fitzgerald PG (2008) Can microplate rotation drive subduction inversion? Geology 36:823–826

Welke B, Licht K, Hennessy A, Hemming S, Pierce Davis E, Kassab C (2016) Applications of detrital geochronology and thermochronology from glacial deposits to the Paleozoic and Mesozoic thermal history of the Ross Embayment, Antarctica. Geochem Geophys Geosyst 17:2762–2780

Wellman H (1979) An uplift map for the South Island of New Zealand, and a model for uplift of the Southern Alps. Royal Soc New Z Bull 18:13–20

Wightman RH, Little TA (2007) Deformation of the Pacific Plate above the Alpine Fault ramp and its relationship to expulsion of metamorphic fluids: an array of backshears. In: Okaya D, Stern T, Davey F (eds) A Continental Plate Boundary: Tectonics at South Island, New Zealand, vol 175. American Geophysical Union, Washington DC, pp 177–205

Wildman M, Cogné N, Beucher R (2018) Fission-track thermochronology applied to the evolution of passive continental margins. In: Malusà MG, Fitzgerald PG (eds) Fission-track thermochronology and its application to geology. Springer

Willett S, Beaumont C, Fullsack P (1993) Mechanical model for the tectonics of doubly vergent compressional orogens. Geology 21:371–374

Yamato P, Burov E, Agard P, Le Pourhiet L, Jolivet L (2008) HP-UHP exhumation during slow continental subduction: self-consistent thermodynamically and thermomechanically coupled model with application to the Western Alps. Earth Planet Sci Lett 271:63–74

Zattin M, Andreucci B, Thomson SN, Reiners PW, Talarico FM (2012) New constraints on the provenance of the ANDRILL AND 2A succession (western Ross Sea, Antarctica) from apatite triple dating. Geochem Geophys Geosyst 13

Zeitler PK, Chamberlain CP, Smith HA (1993) Synchronous anatexis, metamorphism, and rapid denudation at Nanga Parbat (Pakistan Himalaya). Geology 21:347

Zhao L, Paul A, Guillot S, Solarino S, Malusà MG, Zheng T, Aubert C, Salimbeni S, Dumont T, Schwartz S (2015) First seismic evidence for continental subduction beneath the Western Alps. Geology 43:815–818

Zirakparvar NA, Baldwin SL, Vervoort JD (2011) Lu-Hf garnet geochronology applied to plate boundary zones: insights from the (U)HP terrane exhumed within the Woodlark Rift. Earth Planet Sci Lett 309:56–66

Zirakparvar NA, Baldwin SL, Schmitt AK (2014) Zircon growth in (U) HP quartzo-feldspathic host gneisses exhumed in the Woodlark Rift of Papua New Guinea. Geochem Geophys Geosyst 15:1258–1282

Zirakparvar NA, Baldwin SL, Vervoort JD (2012) The origin and evolution of the Woodlark Rift of Papua New Guinea. Gondwana Res. https://doi.org/10.1016/j.gr.2012.06.013

Zwart HJ (1979) The geology of the Central Pyrenees. Leidse Geol Mededelingen 50:1–74